



รายงานวิจัยฉบับสมบูรณ์

โครงการ การวิเคราะห์พฤติกรรมการถ่ายเทความร้อนและการไหลในวัสดุ
พรุนอิ่มตัวแบบหลายชั้นที่ได้รับพลังงานความร้อนจากคลื่นไมโครเวฟโดยใช้
ท่อนำคลื่นทรงสี่เหลี่ยม

โดย ผู้ช่วยศาสตราจารย์ ดร. วาทิต ภักดี และศาสตราจารย์ ดร. ผดุงศักดิ์ รัตนเดโช

รายงานวิจัยฉบับสมบูรณ์

โครงการ การวิเคราะห์พฤติกรรมการถ่ายเทความร้อนและการไหลในวัสดุ
พรุนอิ่มตัวแบบหลายชั้นที่ได้รับพลังงานความร้อนจากคลื่นไมโครเวฟโดยใช้
ท่อนำคลื่นทรงสี่เหลี่ยม

คณะผู้วิจัย

สังกัด

- 1) ผู้ช่วยศาสตราจารย์ ดร. วาทิต ภักดี คณะวิศวกรรมศาสตร์ ม. ธรรมศาสตร์
- 2) ศาสตราจารย์ ดร. ผดุงศักดิ์ รัตนเดโช คณะวิศวกรรมศาสตร์ ม. ธรรมศาสตร์

สนับสนุนโดยสำนักงานกองทุนสนับสนุนการวิจัย

(ความเห็นในรายงานนี้เป็นของผู้วิจัย สกว. ไม่จำเป็นต้องเห็นด้วยเสมอไป)

บทคัดย่อ

งานวิจัยนี้จะศึกษาการถ่ายเทความร้อนในวัสดุพรุนอิ่มตัวที่ได้รับพลังงานจากคลื่น ไมโครเวฟโดยวัสดุพรุนมีลักษณะเป็นแบบหลายชั้น (multi-layered) ซึ่งกล่าวได้ว่ามีการกระจาย ของความพรุนที่ไม่สม่ำเสมอ โดยมุ่งเน้นการศึกษาโดยอาศัยพื้นฐานทางทฤษฎีในโครงสร้าง ระดับจุลภาค (microscopic level) เพื่อพัฒนาแบบจำลองทางคณิตศาสตร์ของการถ่ายเทความ ร้อนเพื่อทำนายและศึกษาพฤติกรรมการถ่ายเทความร้อน, ตัวแบบ Brinkmann-Forchheimer ถูกนำมาใช้เพื่อคำนวณพฤติกรรมการไหลผ่านวัสดุพรุน และใช้ Maxwell's equations สำหรับ คำนวณการกระจายตัวของสนามแม่เหล็กไฟฟ้าโดยระเบียบวิธี finite difference time domain (FDTD) คำตอบทั้งหมดที่เปลี่ยนแปลงตามเวลาคำนวณโดยอาศัยวิธี SIMPLE การเปลี่ยนแปลง พารามิเตอร์ที่เกี่ยวข้อง, การกระจายตัวของอุณหภูมิ และลักษณะการเคลื่อนตัวของของไหลใน ช่องว่างของรูพรุนอันเนื่องมาจากความร้อนที่เกิดขึ้นภายในจากพลังงานคลื่นไมโครเวฟ ศึกษา ถึงรูปแบบการใหลของของเหลวในวัสดุพรุนและลักษณะการกระจายตัวของความร้อนในชิ้น ทดสอบซึ่งจำลองเป็นวัสดุพรุนโดยใช้ลูกแก้ว (glass beads) และน้ำที่แทรกตัวในช่องว่าง ระหว่างลูกแก้วซึ่งบรรจุในกล่อง (packed bed) ที่ได้รับคลื่นไมโครเวฟความถี่ 2.45 GHz ที่ โหมด TE₁₀ในท่อนำคลื่นทรงสี่เหลี่ยม จากผลการวิจัยพบว่า จากการเปรียบเทียบผลการ คำนวณกับผลจากการทดลอง ตัวแบบที่นำเสนอสามารถทำนายพฤติกรรมการถ่ายเทความร้อน ในวัสดุพรุนได้อย่างถูกต้อง และความไม่สม่ำเสมอของค่าความพรุนมีผลต่อการไหลของมวลสาร และการถ่ายเทความร้อนในวัสดุพรุนอย่างมีนัยสำคัญ องค์ความรู้ที่ได้รับจากงานวิจัยชิ้นนี้มี ประโยชน์อย่างสูงต่ออุตสาหกรรมต่างๆมากมาย รวมไปถึงเทคโนโลยีการการเก็บรักษาเนื้อเยื่อ นอกจากนี้องค์ความรู้ดังกล่าวยังสามารถนำไปช่วยวิเคราะห์เชิงลึก ในงานด้านการแพทย์ สำหรับปัญหาที่มีการเปลี่ยนสถานะของสสาร อาทิเช่น ปัญหาการเย็นเยือกในวัสดุพรุน (freezing in porous media) และปัญหาการทำละลายในวัสดุพรุน (melting in porous media) เป็นต้น

Abstract

The transient natural convection flow through a fluid-saturated porous medium in a square enclosure with a partial convection condition was investigated using Brinkmann-extended Darcy model. Physical problem consists of a rectangular cavity filled with porous medium. The cavity is insulated except the top wall that is partially exposed to an outside ambient. The exposed surface allows convective transport through the porous medium, generating a thermal stratification and flow circulations. The formulation of differential equations is nondimensionalized and then solved numerically under appropriate initial and boundary conditions. The finite difference equations handling the convection boundary condition of the open top surface are derived. In

addition to the negative density gradient in the direction of gravitation, a lateral temperature gradient in the region close to the top wall induces the buoyancy force under an unstable condition. The two-dimensional flow is characterized mainly by the clockwise and anti-clockwise symmetrical vortices driven by the effect of buoyancy. Unsteady effects of associated parameters were examined. The modified Nusselt number (Nu) is systematically derived. This newly developed form of Nu captures the heat transfer behaviors reasonably accurately. It was found that the heat transfer coefficient, Rayleigh number, Darcy number as well as flow direction strongly influenced characteristics of flow and heat transfer mechanisms. Thereafter, the microwave heating of a porous medium with a non-uniform porosity is numerically investigated, based on the proposed numerical model. A two-dimensional variation of porosity of the medium is considered. The generalized non-Darcian model developed takes into account of the presence of a solid drag and the inertial effect. The transient Maxwell's equations are solved by using the finite difference time domain (FDTD) method to describe the electromagnetic field in the wave guide and medium. The temperature profile and velocity field within a medium are determined by the solution of the momentum, energy and Maxwell's equations. The coupled non-linear set of these equations are solved using the SIMPLE algorithm. In this work, a detailed parametric study is conducted for a heat transport inside a rectangular enclosure filled with saturated porous medium of constant or variable porosity. The numerical results agree well with the experimental data. Variations in porosity significantly affect the microwave heating process as well as convective flow pattern driven by microwave energy.

Project Code : สัญญาเลขที่ MRG5180238

Project Title: การวิเคราะห์พฤติกรรมการถ่ายเทความร้อนและการไหลวัสดุพรุนอิ่มตัวแบบ หลายชั้นที่ได้รับพลังงานความร้อนจากคลื่นไมโครเวฟโดยใช้ท่อนำคลื่นทรงสี่เหลี่ยม

Investigator : ชื่อนักวิจัย และสถาบัน

ผู้ช่วยศาสตราจารย์ ดร. วาทิต ภักดี และ ศาสตราจารย์ ดร.ผดุงศักดิ์ รัตนเดโช ภาควิชาวิศวกรรมเครื่องกล คณะวิศวกรรมศาสตร์ มหาวิทยาลัยธรรมศาสตร์

E-mail Address: pwatit@engr.tu.ac.th

Project Period : 15 พฤษภาคม 2551 —15 พฤษภาคม 2553

วัตถุประสงค์

In the first part of this work, the quantitative study in terms of Nu is taken into account. The new formulation of Nu is developed to correctly capture heat transfer behaviors. The study of heat transfer due to cooling condition has been carried out for transient natural convective flow in a fluid-saturated porous medium filled in a square cavity. The top surface is partially open to the ambient, allowing the surface temperature to vary, depending on the influence of convection heat transfer mechanism. Computed results are depicted using temperature, flow distributions and heat transfer rates in terms of local and average Nusselt numbers. The influences of associated parameters such as heat transfer coefficient, Rayleigh number and Darcy number on the flow and thermal configurations were examined.

In the second fold, we propose the numerical model for the microwave heating of a saturated porous packed bed in which the porosity variation is considered. The non-Darcian boundary and inertial effects are taken into account. Heating characteristic and flow pattern are numerically investigated. The numerical model is validated with an experimental data obtained using a rectangular waveguide operated under the microwave of TE₁₀ mode.

วิธีทดลอง

We carried out the numerical approach and validate the numerical scheme by comparing the computed results with experimental data. The experiment apparatus of microwave heating of saturated porous medium using a rectangular wave guide used is shown in figure 1. The microwave system is a monochromatic wave of TE_{10} mode operating at a frequency of 2.45 GHz. From figure 1(b), magnetron (no.1) generates microwave and transmits along the z-direction of the rectangular wave guide (no.5) with inside cross-sectional dimensions of $109.2 \times 54.61 \text{ mm}^2$ that refers to a testing area (red circle) and a water load (no. 8) that is situated at the end of the wave guide. On the upstream side of the sample, an isolator is used to trap any microwave reflected from the sample to prevent damaging to the magnetron. The powers of incident, reflected and transmitted waves are measured by a wattmeter using a directional coupler (no. 6) (MICRO DENSHI., model DR-5000). Fiberoptic (no. 7) (LUXTRON Fluroptic Thermometer., model 790, accurate to $\pm 0.5^{\circ}$ C) is employed for temperature measurement. The fiberoptic probes are inserted into the sample, and situated on the

XZ plane at Y = 25 mm. (see in Figure 2). Due to the symmetrical condition, temperatures are measured for only one side of plane. The samples are saturated porous packed beds that compose of glass beads and water. A container with a thickness of 0.75 mm is made of polypropylene which does not absorb microwave energy.

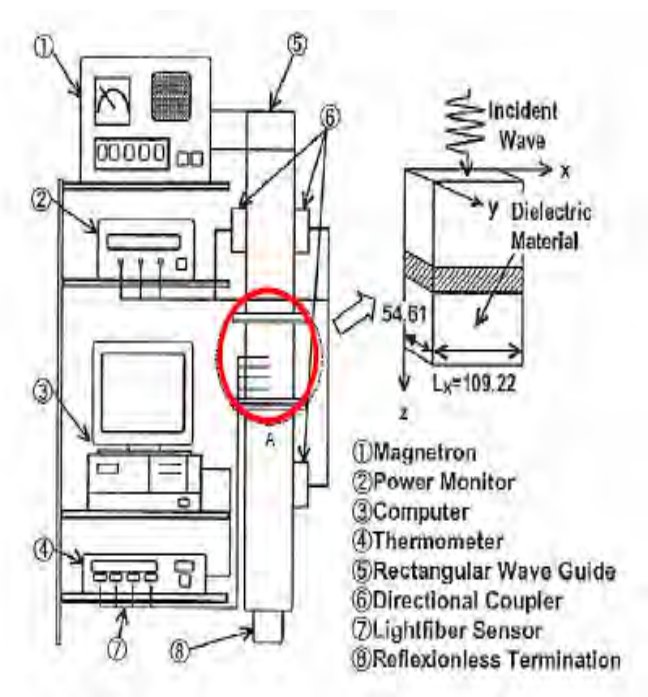


Figure 1. The microwave heating system with a rectangular wave guide.

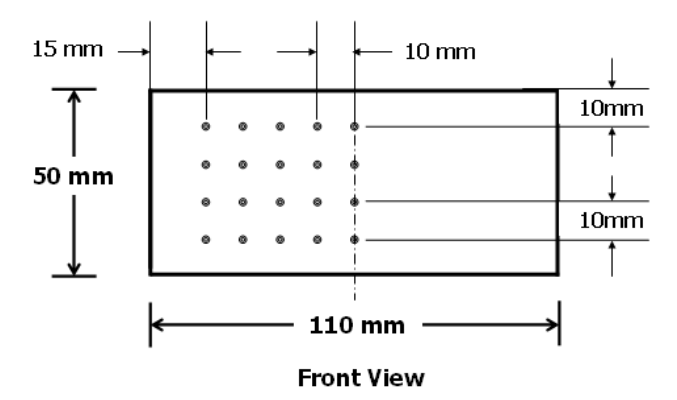


Figure 2. Locations of temperature measurement in symmetrical xz plane.

In our present experiment, a glass bead 0.15 mm in diameter is examined. The averaged (free stream) porosity of the packed bed corresponds to 0.385. The dielectric and thermal properties of water, air and glass bead are listed in Table 1.

Table 1 Electromagnetic and thermo physical properties used in the computations [1]

Property	water	Glass
----------	-------	-------

		bead
Heat capacity, $C_p(Jkg^{-1}K^{-1})$	4190	800
Thermal conductivity,	0.609	1.0
$\lambda \left(Wm^{-1}K^{-1}\right)$		
Density, $ ho\!\!\left(\!kgm^{-3}\right)$	1000	2500
Dielectric constant 1 , $\varepsilon_{r}^{'}$	$88.15-0.414T+(0.131\times10^{-2})T^{2}-(0.046\times10^{-4})T^{3}$	5.1
Loss tangent ¹ , $\tan \delta$	$0.323-(9.499\times10^{-3})T+(1.27\times10^{-4})T^{2}-(6.13\times10^{-7})T^{3}$	0.01

¹ T is in °C.

In terms of numerical implementation, the description of heat transport and flow pattern of liquid layer equations requires specification of temperature (T), velocity component (u, w) and pressure (p). These equations are coupled to the Maxwell's equations by the heating effect of the microwaves in the liquid-container domain.

4.1 Electromagnetic equations and FDTD discretization

The electromagnetic equations are solved by using FDTD method. With this method the electric field components (E) are stored halfway between the basic nodes while magnetic field components (H) are stored at the center. So they are calculated at alternating half-time steps. E and H field components are discretized by a central difference method (second-order accurate) in both spatial and time domain.

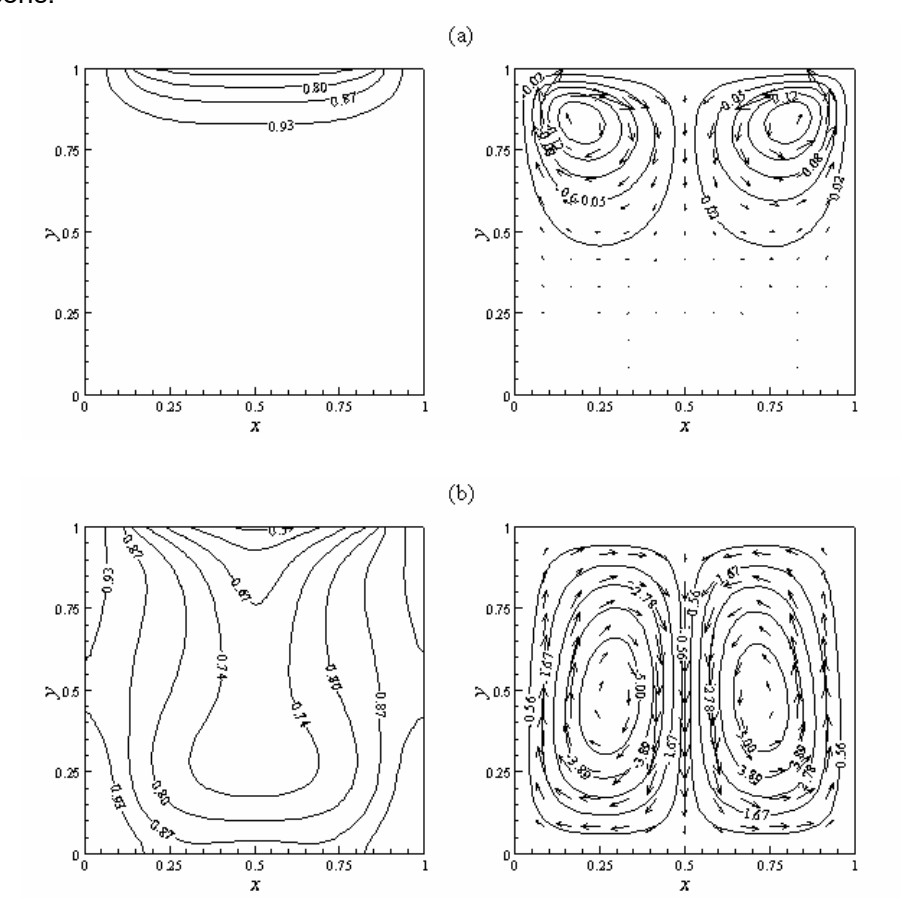
4.2 Fluid flow and heat transport equations and finite control volume discretization

The governing equations are solved numerically by using the finite control volume along with the SIMPLE algorithm developed by Patankar [2]. The reason to use this method is advantages of flux conservation that avoids generation of parasitic source. The basic strategy of the finite control volume discretization method is to divide the calculated domain into a number of control volumes and then integrate the conservation equations over this control volume over an interval of time [t, $t+\Delta t$]. At the boundaries of the calculated domain, the conservation equations are discretized by integrating over half the control volume and taking into account the boundary conditions. At the corners of the calculated domain we used a quarter of control volume. The fully Euler implicit time discretization finite difference scheme is used to arrive at the solution in time.

Additionally, the details about numerical discretization of this method can be found in the recent literature.

ผลการทดลองและวิจารณ์ผล

The following discussions were extracted from [3-4] which include the numerical results from the present study, which focuses on transient flow and thermal behaviors. Initial values of θ for an entire domain are set to 1, as the ambient temperature is lower than temperature of the medium in cavity. The investigations were conducted for a range of controlling parameters, which are Darcy number (Da) Rayleigh number (Ra) and convective heat transfer coefficient (h). The uniform porosity ε of 0.8 and unity aspect ratio (A=1) were considered throughout in the present study. In order to assess global effects of these parameters, the streamlines and isotherm distributions inside the entire cavity are presented. All the figures have the same range of contour levels to facilitate direct comparisons.



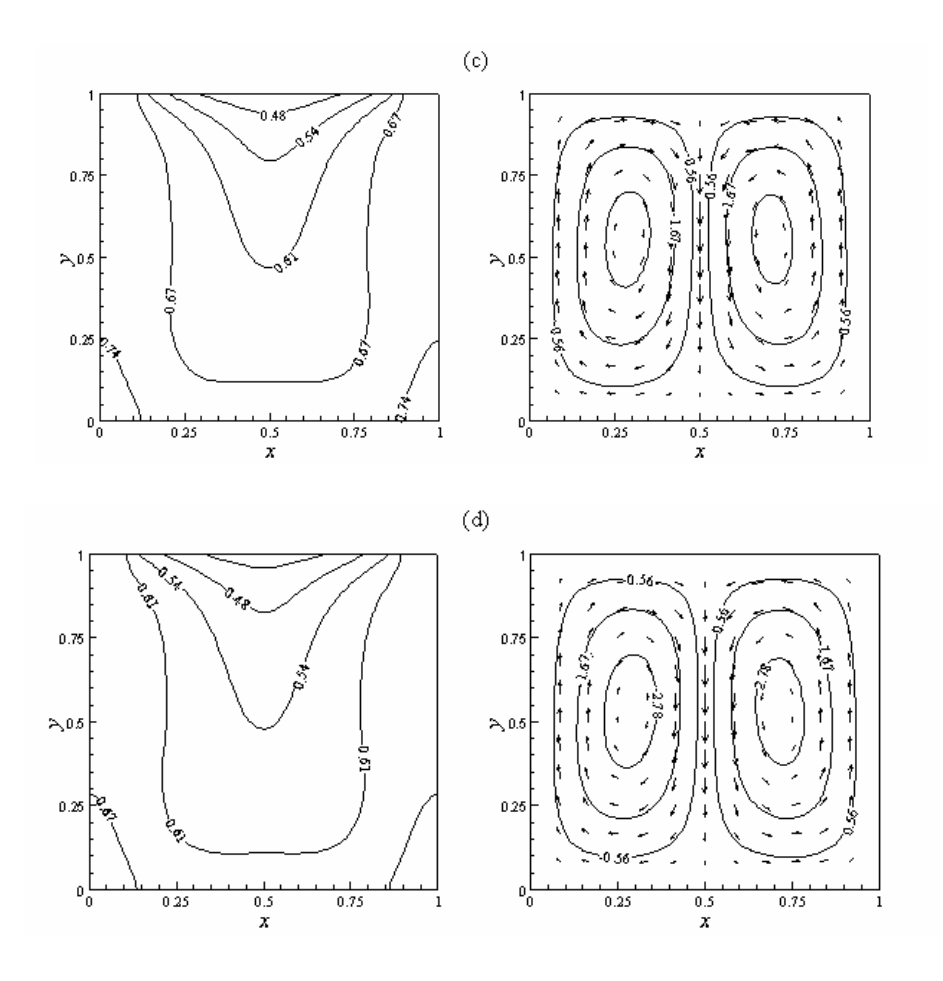
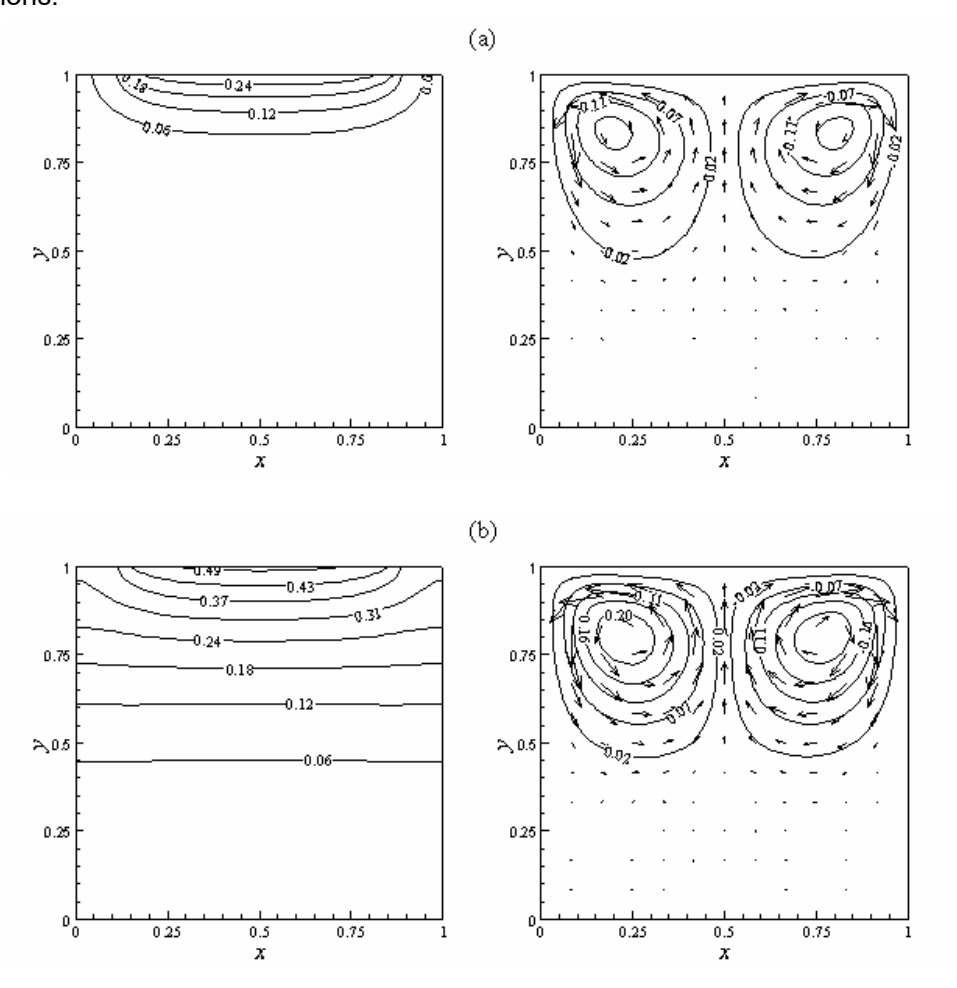


Figure 3. Sequential files with the cooling boundary for contours of temperature and streamlines at times τ = (a) 0.013, (b) 0.088, (c) 0.168, and (d) 0.245. (Ra = $5x10^4$, Da = 0.1, Pr =1.0, ε = 0.8, and h = 60 W/m²K)

The resulting computational fields were extracted at the time adequately long to ensure sufficient energy transferred throughout the domain. Figure 3 displays instantaneous images of the contour plots during the thermal and flow evolution. The Rayleigh number of $5x10^4$, Da = 0.1, Pr = 1.0, h = 60 w/m 2 K, and ε =0.8 are considered. The two columns represent contours of temperature and stream function respectively from left to right. With the same contour levels, comparisons can be made directly. The four snapshots from top to bottom in each column are results taken at the dimensionless times τ = 0.013, 0.088, 0.168, and 0.245. The vertical temperature stratification is observed. The streamline contours exhibit circulation patterns, which are characterized by the two symmetrical vortices. The fluid flows as it is driven by the effect of buoyancy. This effect is distributed from the top wall of cavity where the fluid is cooled through the partially open surface, causing lower temperature near the top boundary. The existence of the non-uniform temperature along the top surface, and a decrease of density in the direction of

gravitational force lead to an unstable condition. Thus the buoyancy effect is associated with the lateral temperature gradients at locations near the top surface. High temperature portions of fluid become lighter than the lower temperature portions at the middle where the wall is open. Theses light portions from two sides then expand laterally towards the center, compressing the lower temperature portions, which are heavier. As a result, the downward flows along the vertical centerline are originated, while the lighter fluid will rise, cooling as it moves. Consequently, the circulation flow pattern is generated. The clockwise and counterclockwise circulations are located respectively on the left side and right side within the enclosure. The circulations get larger and expand downward with time. An increase in strength of the vortices develops fast during early simulation times, and its maximum magnitude reaches 6.0. Subsequently the vortices are weakened. Similarly, temperature distribution progressively evolves relatively fast in the early times. Slow evolution is observed after that. This result corresponds well with the decrease in strength of flow circulations.



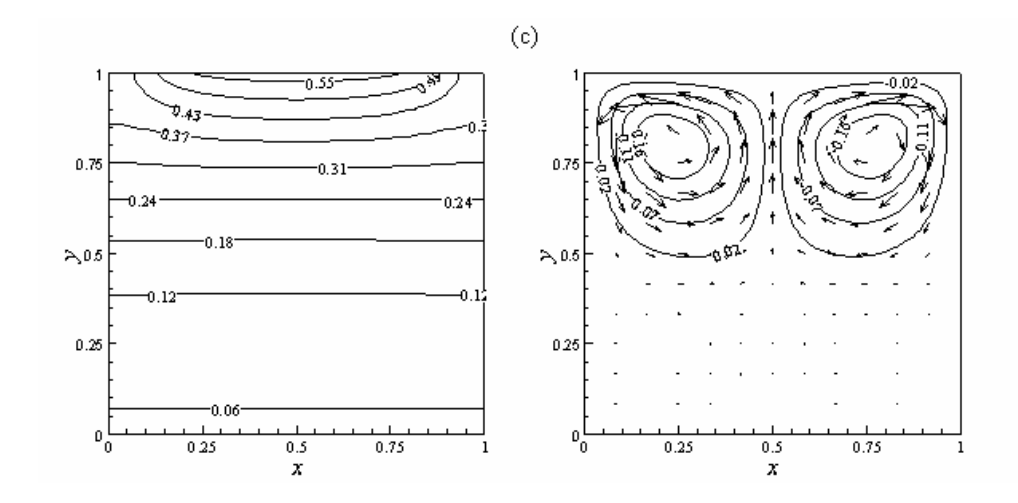


Figure 4. Sequential files with the heating boundary for contours of temperature and streamlines at times τ = (a) 0.013, (b) 0.088, and (c) 0.168. (Ra = $5x10^4$, Da = 0.1, Pr = 1.0, ε = 0.8, and h = 60 W/m²K)

The resulting computational fields of the heating scenario were demonstrated in figure 4. For a purpose of comparison the parameter set remains unchanged. Similarly, the two columns represent temperature and stream function taken at the dimensionless times τ = 0.013, 0.088, and 0.168. The vertical temperature stratification is observed. The streamline contours exhibit circulation patterns, which are characterized by the two symmetrical vortices. The fluid flows as it is driven by the effect of buoyancy. This effect is distributed from the top wall of cavity where the fluid is heated through the partially open area. Unlike the cooling case, in which a presence of negative density mainly causes an unstable condition, in the heating case the lateral density gradient near the top surface is the only cause to the unstable condition that actually leads to the buoyancy force. This reason explains why the heated circulations are weaker than the cooled circulations presented earlier. Heated portions of the fluid become lighter than the rest of fluid, and are expanded laterally away from the center to the sides then flow down along the two vertical walls, leading to the counter-clockwise and clockwise flow circulations. These results suggest that the buoyancy forces are able to overcome the retarding influence of viscous forces. It should be noted that directions of circulations are opposite to those under cooling condition. An increase in strength of the vortices develops fast during early simulation times, and its maximum magnitude reaches 0.25, which is considerably small. Therefore, profiles of temperature contours look similar to those for a stationary fluid, in which the heat transfer is caused by conduction. Similarly, temperature distribution progressively evolves relatively fast in the early times. This result corresponds to the decrease in strength of flow circulations. In the remaining area, the fluid is nearly stagnant suggesting that conduction is dominant due to minimal flow activities. This is because of strong viscous effects. It is evident from figures 1 and 2 that the cooling case reveals a considerably faster thermal evolution thereby greater convection rate. Furthermore, heat transfer in the vertical direction is much greater than that in the span wise direction. The reader is directed to [5] for more detailed discussions of heating configuration.

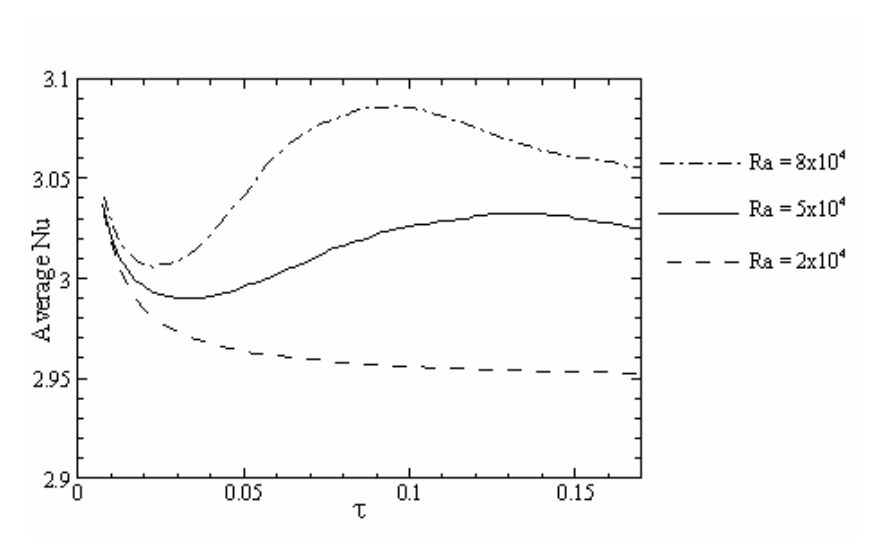


Figure 5.Variations of the average Nusselt number with time for different Rayleigh numbers. (Da = 0.01, h = 60 W/m 2 K, Pr = 1.0, and ε = 0.8)

Figure 5 presents how the average Nusselt number changes with time for a variety of Rayleigh numbers. The local Nu at the open portion on the top boundary is computed according to the developed equation. The average Nusselt number \overline{Nu} is then obtained accordingly. At first, the value of \overline{Nu} decreases rapidly for all cases of Rayleigh numbers, clearly due to the fast reduction of temperature gradients. In the case of low Rayleigh number of $2x10^4$, \overline{Nu} progressively decreases with time. While for higher Ra $(5x10^4, 8x10^4)$, \overline{Nu} values become greater and reach peak values after some time. Further increasing Ra $(8x10^4)$, higher maximum Nu is reached more quickly due to greater flow intensities. At late simulation times when stable state is approached, the values of \overline{Nu} continually decrease and essentially level off at late times, thereby diminishing heat transfer by means of heat convection. It can be expected that \overline{Nu} will continue to decrease with time as the steady state is reached.

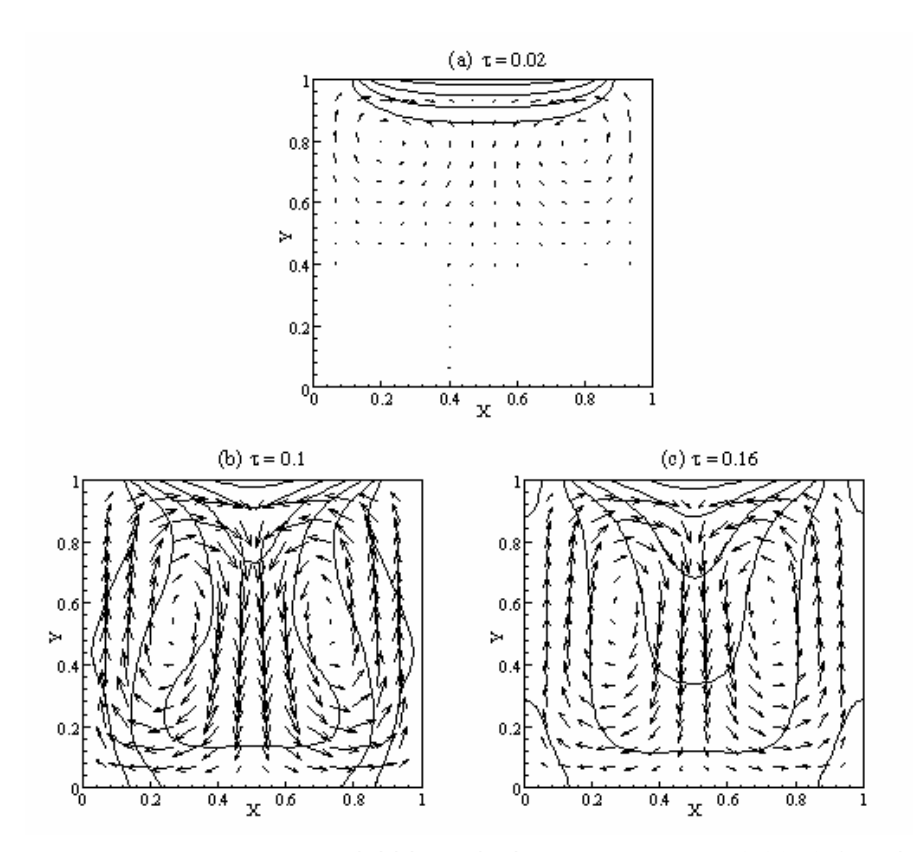


Figure 6. temperature contours overlaid by velocity vectors at $\tau = 0.02$, 0.1 and 0.16 respectively. Data is taken from that of figure 5 for Ra = $8x10^4$.

To gain insights into the observation made, the local values of the corresponding thermal and flow behaviors were traced for Ra of $8x10^4$. The data are extracted and depicted in figure 6 at τ of 0.02, 0.1 and 0.16. The streamlines and isotherms are illustrated in figure 6a-c at $\tau=0.02$, 0.1 and 0.16 respectively. At $\tau=0.02$, the averaged Nu is small due to minimal flow activities. Then \overline{Nu} gets higher as the flows gets stronger, which can be seen in figure 6(b) at $\tau=0.1$. The effect of the rigorous flows overcomes the continual reduction of temperature gradient, resulting in the increase in \overline{Nu} . At the subsequent times, the viscous effect increasingly weakens the flows as shown in figure 6(c). As a result, the reduction of temperature gradient prevails, causing \overline{Nu} to decrease. These results correspond well with the variation with time of the averaged Nu, depicted in figure 7. The results confirm the validation of the proposed formulation of Nu.

In the present simulations, the formulation that computes the variation of porosity in two directions is employed to describe the two-dimensional porosity variation. The glass bead diameters of 1.0 mm and 3.0 mm are examined with which the free-stream porosity is 0.385. The resulting calculations are illustrated in figure 7 on the x-z plane. Variations of the bed porosity were considered since it was proved that the

porosity decayed from the wall [6–7]. As clearly seen in the figure, the porosity is high in the vicinity of an impermeable boundary and reduces to a free-stream value at about four to five bead diameters from the boundary [8]. The computed porosities vary accounting to the distances from the walls in two directions. Porosities are largest at the corners because it is not efficient to pack spherical beads at bed corners. The gradients of porosity are found lower with larger particle diameter.

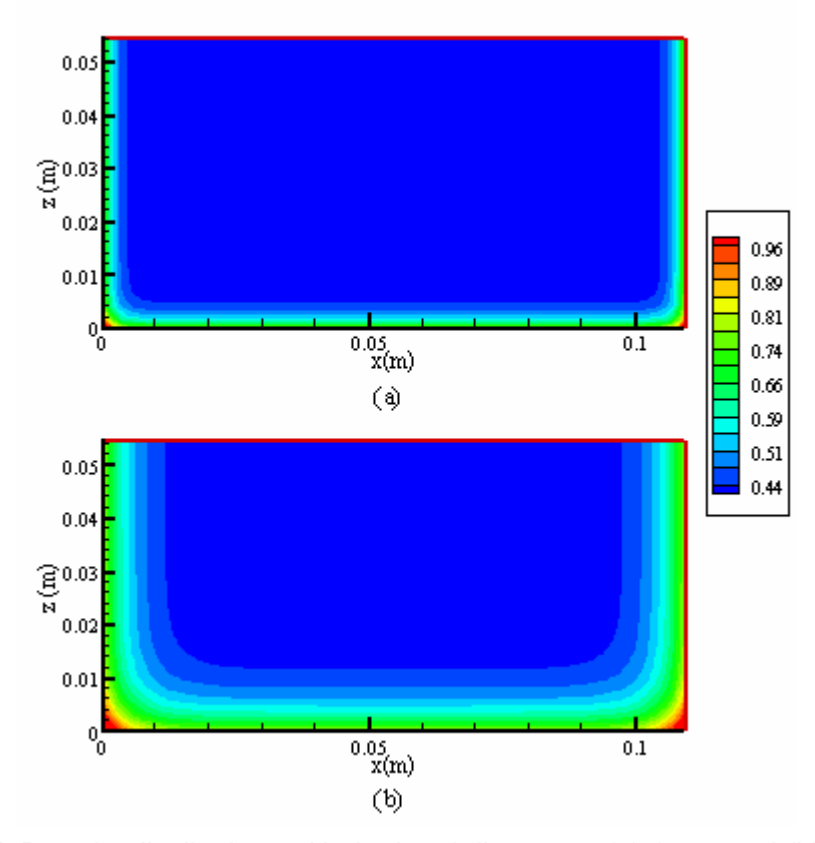


Figure 7. Porosity distributions with the bead diameters: (a) 1 mm and (b) 3 mm.

To examine the validity of the mathematical model, the numerical results were compared with the experimental data. The diameter of glass beads and free-stream porosity are 0.15 mm and 0.385 respectively. With respect to the model simulation, the computed data, for both uniform and non-uniform, cases were extracted at 30 and 50 seconds. The comparisons of temperature distributions on the x-z plane at the horizontal line z=21 mm are shown in Figure 8 at 50 seconds respectively. The results show an appreciably improved agreement when variation of porosity within the packed bed is considered. For the uniform case, the peak temperature is about 40 $^{\circ}$ C at 30 seconds, and reaches 50 $^{\circ}$ C at later time while temperatures are lower in the case of variable porosity. However, it is clear that temperature is highest at the middle location

since the density of the electric field in the TE10 mode is high around the center region in the wave guide.

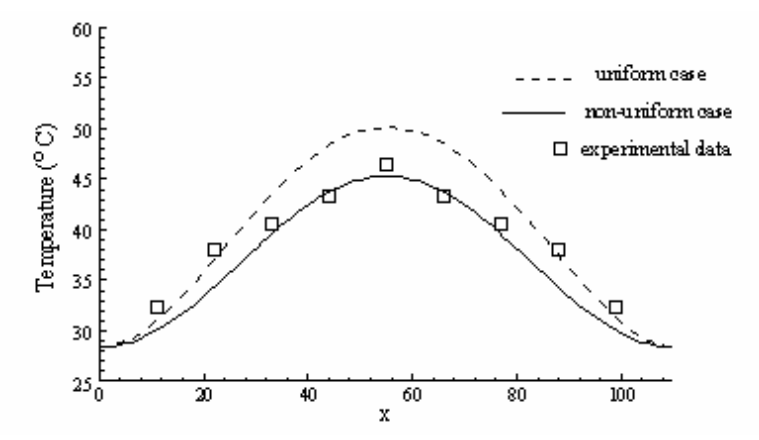


Figure 8. The temperature distributions taken at 50 seconds are shown as to compare the numerical solutions with the experimental result.

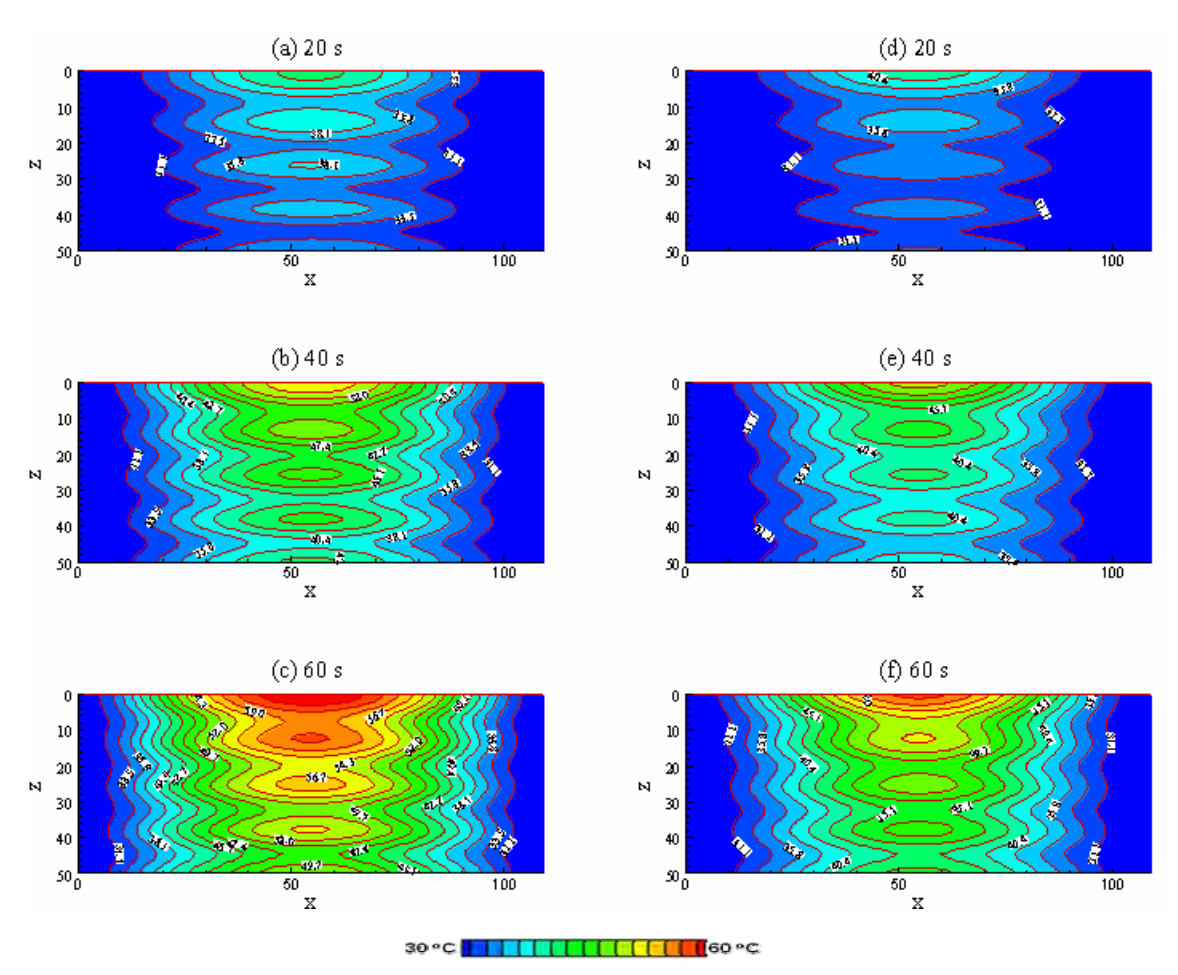


Figure 9. Time evolutions of temperature contour within the porous bed at 20, 40 and 60 seconds for uniform case (a-c) and non-uniform case (d-f).

Figure 9 displays temperature contours as a function of time of the two cases which exhibit a wavy behavior corresponding to the resonance of electric field. For the

non-uniform porosity, the heating rate is noticeably slower than that for the uniform porosity. The reason behind this is that in the non-uniform porosity medium, more water content exists near the bottom wall attributed to a higher water-filled pore density. Since water is very lossy, large amount of energy can be absorbed as both the incoming waves and the reflected waves attenuate especially at the bottom area. This occurrence results in a resonance of weaker standing wave with smaller amplitude throughout the packed bed. The weaker standing wave dissipates less energy which is in turn converted into less thermal energy, giving relatively slow heating rate. This explains why non-uniform porous gives overall lower temperature. Furthermore, more amount of water present in the non-uniform medium causes a smaller depth of penetration since water has relatively high values of dielectric constant and high loss tangent. Figure 10 shows variation of centerline temperature vertically along the z axis at the different times of the two bed types. The resulting plots confirm wavy behavior shown in figure 9. Moreover, it is obvious that the bed temperature is higher in the uniform-porosity porous bed.

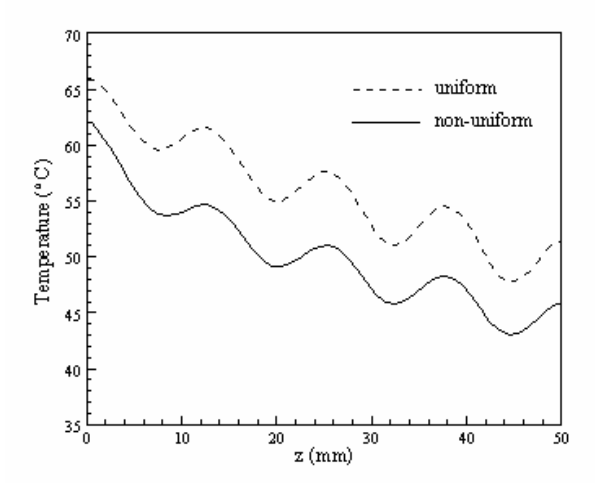


Figure 10. Centerline temperature along the z axis for uniform (dashed line) and non-uniform (solid line) porous packed bed.

In terms of flow characteristic, the instantaneous velocity vectors at 60 seconds are displayed in figure 11. The fluid flows as it is driven by the effect of buoyancy that overcomes the retarding viscous force. The non-uniform temperature distribution evident in figure 9 leads to an unstable condition. Temperature gradients which exist in both transverse and axial directions result in circulated flows. The velocities are higher close to the top boundary since there exist higher temperature gradients thereby higher density gradients leading stronger buoyancy-induced flows. It is seen that flow velocities in the variable-porosity medium are lower than those in the uniform-porosity medium.

This result is attributed to higher porosities near walls in the non-uniform case. Higher porosity medium corresponds to higher permeability which allows greater flow velocity due to smaller boundary and inertial effects. The difference is clear in the vicinity of walls where high velocities carry energy from the wall towards the inner area.

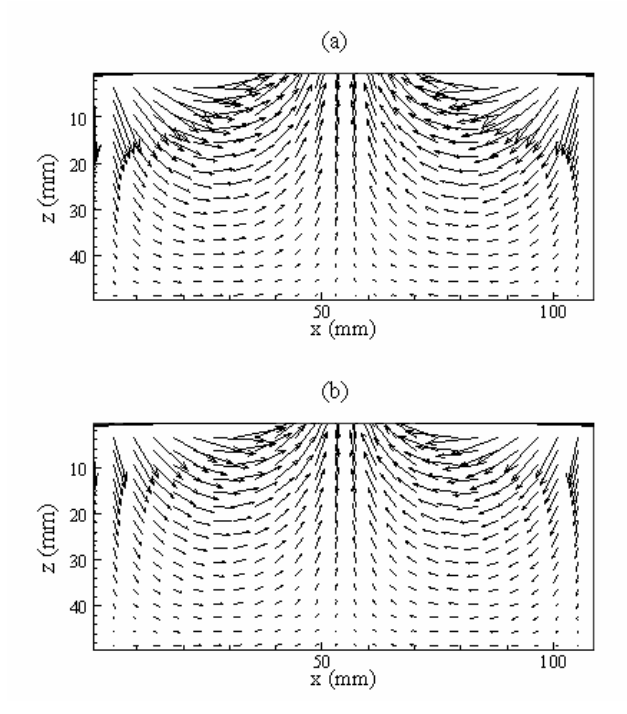


Figure 11. Velocity vectors from the two cases; (a) Non-uniform (b) Uniform.

To gain more insight in flow phenomena, the centerline velocity magnitudes along the x direction are depicted in figure 12. It is clear that the non-uniform porosity gives larger magnitudes. Two peaks are seen spatially in both the cases. The peak values are at the same locations as observed in figure 11. More importantly, the gradient of magnitude is larger in the non-uniform case due to the presence of porosity gradients.

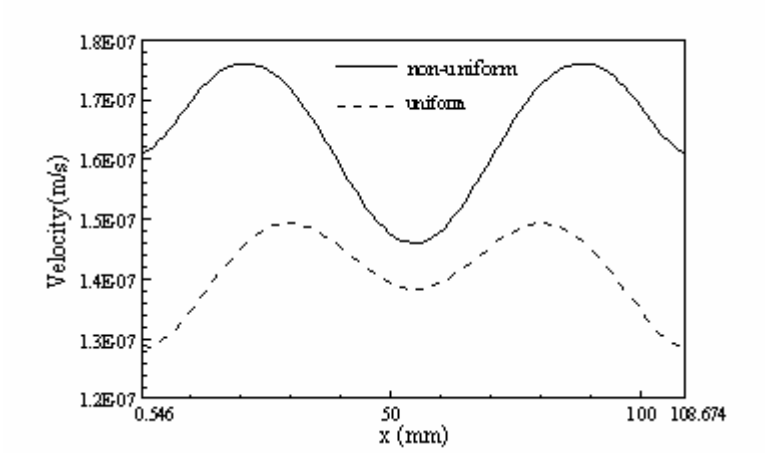


Figure 12. Variations of u-component velocity along the x axis for uniform (dashed line) and non-uniform (solid line) porous packed bed.

สรุป

Numerical simulations of natural convection flow through a fluid-saturated porous medium in a rectangular cavity due to convection at top surface were performed. Transient effects of associated controlling parameters were examined. The twodimensional flow is characterized mainly by two symmetrical eddies that are initiated by the presence of buoyancy effect. In the cooling case, the buoyancy effect is associated not only with the lateral temperature gradient at locations near the top surface, but also with the condition that the density gradient is negative in the direction of gravitational force. On the other hand, the buoyancy force is induced solely by the lateral temperature gradient in the heating case. The cooling and heating flow directions are opposite. Cooling flows are much stronger due to greater buoyancy effects, indicating higher overall convection rate. The heat transfer mechanism is analyzed using the newly derived formulation of Nu. Heat transfer rate is faster around vertical symmetric line relative to the near-wall regions. Large values of Rayleigh number increase streamline intensities, thus enhancing the downward flow penetration. The temperature stratification penetrates deeper toward the bottom wall, and temperature range within the domain is extended. Therefore it enlarges the region where convection mode is significant. Small values of Darcy number hinder the flow circulations. Therefore the heat transfer by convection is considerably suppressed. Furthermore, the new formulation of Nu captures the heat transfer behaviors reasonably correctly.

The microwave heating of a porous medium with a non-uniform porosity is carried out, based on the proposed numerical model. The two-dimensional variation of porosity of the medium is considered to be a function of the distance from the bed walls. The transient Maxwell's equations are employed to solve for the description of the electromagnetic field in the wave guide and medium. The generalized non-Darcian model that takes into account of the presence of a solid drag and the inertial effect is included. The numerical results are in a good agreement with the experimental data. In addition to the effect on the convective flow velocity that is larger in the non-uniform case, it is found that the variation of porosity near the wall has an important influence on the dielectric properties of the porous packed bed that affect the heating process markedly.

เอกสารอ้างอิง

- [1] P. Ratanadecho, K. Aoki, M. Akahori, Experimental and Numerical study of microwave drying in unsaturated porous material, International Communications in Heat and Mass Transfer 28 (5) (2001) 605-616.
- [2] S. V. Patankar, Numerical Heat Transfer and Fluid Flow, Hemisohere, New York, 1980.
- [3] W. Pakdee, P. Rattanadecho, Numerical Analysis of Natural Convection in Porous Cavity with Partial Convective Cooling Condition, *Journal of Porous Media 2009*, Vol.12, pp. 1083-1100.
- [4] W. Pakdee, P. Rattanadecho, Numerical Natural Convection in a Saturated Variable-Porosity Medium due to Microwave Heating, *ASME Journal of Heat Transfer, 2010* (submitted)
- [5] W. Pakdee, P. Rattanadecho, Unsteady Effects on Natural Convective Heat Transfer through Porous Media in Cavity due to Top Surface Partial Convection. *Applied Thermal Engineering* 2006; volume 26, issues 17-18, pages 2316-2326.
- [6] R. F. Benenati, C. B. Brosilow, Void fraction distribution in pack beds AIChE Journal, 8 (1962) 359-361.
- [7] K. Vafai, Convective flow and heat transfer in variable-porosity media, Journal of Fluid Mechanics 147 (1984) 233-259.
- [8] A. Amiri, K. Vafai, Analysis of dispersion effects and non-thermal equilibrium, non-Darcian, variable porosity incompressible flow through porous media, International Journal of Heat and Mass Transfer 37 (6) (1994) 939-954.

ข้อเสนอแนะสำหรับงานวิจัยในอนาคต

งานวิจัยนี้สามารถพัฒนาต่อโดยปรับแบบจำลองคณิตศาสตร์ให้เป็นแบบ 2-equation model ซึ่ง จะแยกการคำนวณทางอุณหพลศาสตร์ของของแข็งและของไหล คำตอบที่คำนวณได้จะมี ความถูกต้องยิ่งขึ้น โดยเฉพาะในกรณีปัญหาการไหลความเร็วสูง

Keywords : จำนวน 3-5 คำ

Microwave heating, Non-uniform porosity, Natural convection, Saturated porous media, Convection boundary condition

Output จากโครงการวิจัยที่ได้รับทุนจาก สกว.

- 1. ผลงานตีพิมพ์ในวารสารวิชาการนานาชาติ (ระบุชื่อผู้แต่ง ชื่อเรื่อง ชื่อวารสาร ปี เล่มที่ เลขที่ และหน้า) หรือผลงานตามที่คาดไว้ในสัญญาโครงการ
- 1.1 W. Pakdee, P. Rattanadecho, Numerical Analysis of Natural Convection in Porous Cavity with Partial Convective Cooling Condition, *J. Porous Media 2009*, Vol.12, pp. 1083-1100.
- 1.2 W. Pakdee, P. Rattanadecho, Numerical Natural Convection in a Saturated Variable-Porosity Medium due to Microwave Heating, *ASME Journal of Heat Transfer*, 2010 (submitted)
- 2. การนำผลงานวิจัยไปใช้ประโยชน์
 - เชิงวิชาการ (มีการพัฒนาการเรียนการสอน/สร้างนักวิจัยใหม่) พัฒนาการเรียนการสอนในวิชา ที่อยู่ในหลักสูตรวิศวกรรมศาสตรมหาบัณฑิต สาขาวิชาวิศวกรรมเครื่องกล ม.ธรรมศาสตร์ ดังนี้
 - วก. 729 พื้นฐานการทำความร้อนด้วยไมโครเวฟ
 - วก. 624 การถ่ายเทความร้อนขั้นสูง
- 3. อื่นๆ (เช่น ผลงานตีพิมพ์ในวารสารวิชาการในประเทศ การเสนอผลงานในที่ประชุม วิชาการ หนังสือ การจดสิทธิบัตร)

Pakdee W., and Rattanadecho P. Numerical model of microwave heating in a saturated non-uniform porosity medium using a rectangular waveguide. Paper no. 705, International Symposium on Engineering, Energy and Environment (ISEEE), 26-27 November 2009, Rayong, Thailand.

<u>ภาคผนวก</u>

- 1. Published article
- 2 Submitted manuscript

Published article

JOURNAL OF POROUS MEDIA

Volume 12, Number 11, 2009

CONTENTS

Dynamic Compaction of Soft Compressible Porous Materials: Experiments on Air-Solid Phase Interaction	19
Application of Soft Porous Materials to a High-Speed Train Track	37
Flow and Diffusion of Chemically Reactive Species over a Nonlinearly Stretching Sheet Immersed in a Porous Medium	53
Effect of Porous Fraction and Interfacial Stress Jump on Skin Friction and Heat Transfer in Flow Through a Channel Partially Filled with Porous Material	65
Numerical Analysis of Natural Convection in Porous Cavities with Partial Convective Cooling Conditions	83
TECHNICAL NOTES	
Criterion for Local Thermal Equilibrium in Forced Convection Flow through Porous Media	03
Analytic Solution for Free Convection in an Open Vertical Rectangular Duct Filled with a Porous Medium	13
Homotopy Perturbation Method for General Form of Porous Medium Equation	21

Journal of Porous Media (ISSN: 1091-028X) is published 12 times per year and is owned by Begell House, Inc, 50 Cross Highway, Redding, Connecticut 06896, Phone (203) 938-1300. USA subscription rate for 2009 is \$961.00. Add \$10.00 per issue for foreign airmail shipping and handling fees for all orders shipped outside the United States or Canada. All subscriptions are payable in advance. Subscriptions are entered on an annual basis, i.e., January to December. For immediate service and charge card sales, please call (203) 938-1300 Monday through Friday 9 AM — 5 PM EST. Orders can be faxed to (203) 938-1304 or mailed to Subscriptions Department, Begell House, Inc. 50 Cross Highway, Redding, Connecticut 06896.

Copyright © 2009 by Begell House, Inc. All rights reserved. Printed in the United States of America. Authorization to photocopy items for internal or personal use, or the internal or personal use of specific clients, is granted by Begell House, Inc. for libraries and other users registered with the Copyright Clearance Center (CCC) Transactional Reporting Service, provided that the base fee of \$35.00 per copy, plus .00 per page is paid directly to CCC, 222 Rosewood Drive, Danvers, MA 01923, USA. For those organizations that have been granted a photocopy license by CCC, a separate system of payment has been arranged. The fee code for users of the Transactional Reporting Service is [ISSN 1091-028X/02 \$35.00 + \$0.00]. The fee is subject to change without notice.

Begell House, Inc.'s consent does not extend to copying for general distribution, for promotion, for creating new works, or for resale. Specific permission must be obtained from Begell House, Inc. for such copying.

This journal contains information obtained from highly regarded sources. Reprinted material is quoted with permission, and sources are indicated. A wide variety of references are listed. Reasonable efforts have been made to publish reliable data and information, but the editor and the publisher assume no responsibility for any statements of fact or opinion expressed in the published papers or in the advertisements.

Indexing and Abstracting: Journal of Porous Media is covered by several services provided by ISI®, including Current Contents®/ Engineering, Computing, and Technology, ISI Alerting ServicesTM, and SCI, Science Citation Index®.

Printed October 16, 2009

Numerical Analysis of Natural Convection in Porous Cavities with Partial Convective Cooling Conditions

W. Pakdee* and P. Rattanadecho

Department of Mechanical Engineering, Faculty of Engineering, Thammasat University, Rangsit Campus, Klong Luang, Pathumtani 12120, Thailand

*E-mail: pwatit@engr.tu.ac.th and wpele95@yahoo.com

ABSTRACT

Transient natural convection flow through a fluid-saturated porous medium in a square enclosure with a partially cooling surface condition was investigated using a Brinkmann-extended Darcy model. The physical problem consists of a rectangular cavity filled with porous medium. The cavity is insulated, except the top wall that is partially exposed to an outside ambient. The exposed surface allows convective transport through the porous medium, generating a thermal stratification and flow circulations. The formulation of differential equations is nondimensionalized and then solved numerically under appropriate initial and boundary conditions using the finite difference method. The finite difference equations handling the convection boundary condition of the open top surface are derived for cooling conditions. In addition to the negative density gradient in the direction of gravitation, a lateral temperature gradient in the region close to the top wall induces the buoyancy force under an unstable condition. The two-dimensional flow is characterized mainly by the clockwise and anti-clockwise symmetrical vortices driven by the effect of buoyancy. The directions of vortex rotation generated under the cooling condition are in the opposite direction as compared to the heating condition. Unsteady effects of associated parameters were examined. The modified Nusselt number (Nu) was systematically derived. This newly developed form of Nu captures the heat-transfer behaviors reasonably accurately. It was found that the heat-transfer coefficient, Rayleigh number, Darcy number, as well as flow direction strongly influenced characteristics of flow and heat-transfer mechanisms.

NOMENCLATURE

specific heat capacity [J/kg K] B coefficient of thermal expansion [1/K] c_p Darcy number [-] Da porosity [-] ε gravitational constant [m/s²] dimensionless vorticity g5 h convective heat-transfer coefficient θ dimensionless temperature $[W/m^2K]$ permeability of porous medium [m²] K H cavity length [m] dynamic viscosity [Pa/s] μ k thermal conductivity of the porous kinematic viscosity [m²/s] V fluid density [kg/m³] medium [W/m K] Pf pressure [Pa] dimensionless time τ p Pr Prandtl number [-] stream function [m²/s] ψ Ra Rayleigh number [-] Ψ dimensionless stream function t time [s] vorticity [s⁻¹] w Ttemperature [C] Subscripts velocity component [m/s] ambient condition u, v00 Cartesian coordinates effective x, ydimensionless Cartesian coordinates X, Yinitial condition and index for a number W cavity width [m] of points in x direction **Greek symbols** index for a number of points in y j thermal diffusivity [m²/s] direction α

1. INTRODUCTION

The convective heating or cooling that causes heat and fluid flows inside a cavity is found in various applications including lakes and geothermal reservoirs, underground water flow, solar collectors, etc. (Bergman et al., 1986). Associated industrial applications include secondary and tertiary oil recovery, growth of crystals (Imberger and Hamblin, 1982), heating and drying processes (Stanish et al., 1986; Rattanadecho et al., 2001, 2002), electronic device cooling, solidification of casting, sterilization, etc. Natural or free convection in a porous medium has been studied extensively. Cheng (1978) provides a comprehensive review of the literature on free convection in fluid-saturated

porous media with a focus on geothermal systems. Under the framework of porous media models, Darcy proposed the phenomenological relation between the pressure drop across a saturated porous medium and the flow rate. The Darcy model has been employed in recent investigations. Bradean et al. (1997) assumed Darcy's law and used a Boussinesq approximation to numerically simulatethe free convection flow in a porous media adjacent to a vertical or horizontal flat surface. The surface is suddenly heated and cooled sinusoidally along its length. The Darcy law with the Boussinesq approximationwas also employed by Bilgenand Mbaye (2001) to study the development of a Be'n-ard cell' in a fluid-saturated porous cavity whose lateral walls were cooled. It was found that

the existence of two convective solution branches is related to the Darcy-Rayleigh and Biot numbers. Recently, a numerical study was conducted to solve the problem of thermosolutal convection within a rectangular enclosure (Bera and Khalili, 2002). The results revealed that anisotropy causes significant changes in Nusselt and Sherwood numbers. Many works of flow in porous media, such as the ones addressed above, have used the Darcy law. Although the Darcy law is applicable to slow flows, it does not account for initial and boundary effects. In the situation when the flow is strong and the solid boundary and viscous effects are not negligible, these effects, termed non-Darcy effects, become important (Khanafer and Chamkha, 1998). Bera et al. (1998) considered double diffusive convection due to constant heating and cooling on the two vertical walls based on a non-Darcy model inclined permeability tensor. Two distinguished modifications of Darcy' law are the Brinkmann and the Forchheimer extensions, which treat the viscous stresses at the bounding walls and the nonlinear drag effect due to the solid matrix, respectively (Nithiarasu et al., 1997). The Darcy-Forchheimer-Brinkman model was used to represent the fluid transport within the porous medium in the investigation of a convective flow through a channel (Marafie and Vafai, 2001). In this work the two-equation model was used to describe energy transport for solid and fluid phase. The Brinkman-extended Darcy model has been considered in the literature (Tong and Subramanian, 1985; Laurat and Prasad, 1987; Kim et al., 2000; Pakdee and Rattanadecho, 2006). The Darcy-Forchheimer model has been used in a number of published works (Beckermann et al., 1986; Lauriat and Prasad, 1989; Basak et al., 2006). In the study of effects of various thermal boundary conditions applied to saturated porous cavities, the conduction-dominant regime is within Da $\leq 10^{-5}$. Nithiarasu et al. (1998) examined the effects of the applied heat-transfer coefficient on the cold wall of the cavity upon flow and heat transfer inside a porous medium. The differences between the Darcy and non-Darcy flow regime are clearly investi-

gated for different Darcy, Rayleigh, and Biot numbers and aspect ratios. Variations in Darcy, Rayleigh, and Biot numbers and aspect ratio significantly affect the natural flow convective pattern.

Natural convection flows with a variety of configurations were investigated for different aspects. Oosthuizen and Patrick (1995) performed numerical studies of natural convection in an inclined square enclosure with part of one wall heated to a uniform temperature and with the opposite wall uniformly cooled to a lower temperature and with the remaining wall portions. The enclosure is partially filled with a fluid and partly filled with a porous medium, which is saturated with the same fluid. The main results considered were the mean heat-transfer rates across the enclosure. Nithiarasu et al. (1997) examined effects of variable porosity on convective flow patterns inside a porous cavity. The flow was triggered by sustaining a temperature gradient between isothermal lateral walls. The variation in porosity significantly affected the natural flow convective pattern. Khanafer and Chamkha (1998) performed a numerical study of mixed convection flow in a lid-driven cavity filled with a fluid-saturated porous media. In this study, the influences of the Richardson number, Darcy number, and the Rayleigh number played an important role in mixed convection flow inside a square cavity filled with a fluid-saturated porous media. Recently, Al-Amiri (2000) performed numerical studies of momentum and energy transfer in a lid-driven cavity filled with a saturated porous medium. In this study, the force convection is induced by sliding the top constant-temperature wall. It was found that the increase in Darcy number induces flow activities, causing an increase in the fraction of energy transport by means of convection. With similar description of the domain configuration, Khanafer and Vafai (2002) extended the investigation to mass transport in the medium. The buoyancy effects that create the flow are induced by both temperature and concentration gradients. It was concluded that the influences of the Darcy number, Lewis number, and buoyancy ratio on thermal

and flow behaviors were significant. Furthermore, the state of the art regarding porous medium models has been summarized in recently published books (Nield and Bejan, 1999; Vafai, 2000; Pop and Ingham, 2001; Basak et al., 2006).

Previous investigations have merely focused on momentum and energy transfer in cavities filled with a saturated porous medium subjected to prescribed temperature and prescribed wall heat flux conditions. However, only a limited amount of numerical and experimental work on momentum and energy transfer in a cavity filled with a saturated porous medium subjected to heat-transfer coefficient boundary conditions at the exposed portion of the top wall has been reported. Moreover, very few published work is pertinent to partially heated or cooled porous media, although they are found in a number of applications, such as in flush-mounted electrical heaters or buildings (Desai et al., 1995; Al-Amiri, 2002; Oztop, 2007). The recent work of Oztop (2007) investigated natural convection in partially cooled and inclined porous enclosures. His study presented the steadystate results within the enclosure of isothermal heated and cooled walls. In our study, the surface is partially cooled under the convective boundary condition, allowing the surface temperature to change with time. The convective cooling condition or so-called condition of the third kind is systematically derived. While the focus of the present study is on the cooling effect, our recently published work (Pakdee and Rattanadecho, 2006) studied the influence of partially heated surfaces on thermal/flow behavior. In this previous work, although the results were qualitatively discussed in detail, no quantitative description of heat transfer in terms of Nusselt number (Nu) was reported. Therefore, in order to gain better insight into the analysis, our present study proposes a new formulation of Nu employed to analyze the heat-transfer behaviors. Moreover, to the best knowledge of the authors, no attention has been paid to transient convection due to surface partial convective cooling.

In the present study, the quantitative study in terms of Nu is taken into account. The new formulation

of Nu is developed to correctly capture heat-transfer behaviors. The study of heat transfer due to cooling conditions has been carried out for transient natural convective flow in fluid-saturated porous medium filled in a square cavity. In contrast to the heating condition, the cooling condition changes the direction of the induced flows. The top surface is partially open to the ambient, allowing the surface temperature to vary depending on the influence of convection heat-transfer mechanism. Computed results are depicted using temperature, flow distributions, and heat-transfer rates in terms of local and average Nusselt numbers. The influences of associated parameters such as Rayleigh number and Darcy number on the flow and thermal configurations are examined.

2. PROBLEM DESCRIPTION

The computational domain depicted in Fig. 1 is a rectangular cavity of size W×H filled with a fluid-saturated porous medium. Aspect ratio of unity (A = 1) is used in the present study. The domain boundary is insulated except the top wall, which is partially exposed to an ambient air. The initial and boundary conditions corresponding to the problem are of the following forms:

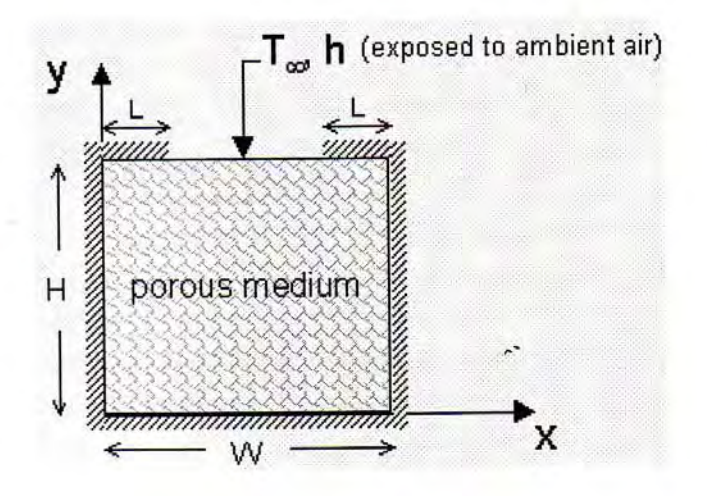


Figure 1. Schematic representation of the computational domain

$$u = v = 0, \quad T = T_i \quad \text{for} \quad t = 0 \tag{1}$$

$$\frac{\partial T}{\partial x} = 0 \text{ at } x = 0, W \qquad 0 \le y \le H$$

$$\frac{\partial T}{\partial y} = 0 \text{ at } y = 0 \qquad 0 \le x \le W$$

$$\frac{\partial T}{\partial y} = 0 \text{ at } y = H \qquad 0 \le x \le L$$
and $W - L \le x \le W$

The boundary condition at the exposed portion of the top wall is defined as

$$-k\frac{\partial T}{\partial y} = h[T - T_{\infty}]$$
 at $y = H$
 $L \le x \le W - L$ (4)

where k and h are effective thermal conductivity and convection heat-transfer coefficient. This type of condition corresponds to the existence of convective heat transfer at the surface and is obtained from the surface energy balance.

The porous medium is assumed to be homogeneous and thermally isotropic. The saturated fluid within the medium is in a local thermodynamic equilibrium (LTE) with the solid matrix (El-Refaee et al., 1998; Nield and Bejan, 1999; Al-Amiri, 2002). The validity regime of local thermal equilibrium assumption has been established (Mohammad, 2000; Marafie and Vafai, 2001). The porous porosity is uniform. The fluid flow is unsteady, laminar, and incompressible. The pressure work and viscous dissipation are all assumed negligible. The thermophysical properties of the porous medium are taken to be constant. However, the Boussinesq approximation takes into account the effect of density variation on the buoyancy force, in which the fluid density is assumed constant except in the buoyancy term of the equation of motion. Furthermore, the solid matrix is made of spherical particles,

while the porosity and permeability of the medium are assumed to be uniform throughout the rectangular cavity. Using standard symbols, the governing equations describing the heat-transfer phenomenon are given by

$$\frac{\partial u}{\partial x} + \frac{\partial v}{\partial y} = 0 \tag{5}$$

$$\frac{1}{\varepsilon} \frac{\partial u}{\partial t} + \frac{u}{\varepsilon^2} \frac{\partial u}{\partial x} + \frac{v}{\varepsilon^2} \frac{\partial u}{\partial y} = -\frac{1}{\varepsilon \rho_f} \frac{\partial P}{\partial x} + \frac{v}{\varepsilon} \left(\frac{\partial^2 u}{\partial x^2} + \frac{\partial^2 u}{\partial y^2} \right) - \frac{\mu u}{\rho_f \kappa} \tag{6}$$

$$\frac{1}{\varepsilon} \frac{\partial v}{\partial t} + \frac{u}{\varepsilon^2} \frac{\partial v}{\partial x} + \frac{v}{\varepsilon^2} \frac{\partial v}{\partial y} = -\frac{1}{\varepsilon \rho_f} \frac{\partial P}{\partial y} + \frac{v}{\varepsilon} \left(\frac{\partial^2 v}{\partial x^2} + \frac{\partial^2 v}{\partial y^2} \right) + g\beta (T - T_{\infty}) - \frac{\mu v}{\rho_f \kappa} \tag{7}$$

$$\sigma \frac{\partial T}{\partial t} + u \frac{\partial T}{\partial x} + v \frac{\partial T}{\partial y} = \alpha \left(\frac{\partial^2 T}{\partial x^2} + \frac{\partial^2 T}{\partial y^2} \right)$$
 (8)

$$\sigma = \frac{\left[\varepsilon(\rho c_p)_f + (1 - \varepsilon)(\rho c_p)_s\right]}{(\rho c_p)_f} \tag{9}$$

where κ is medium permeability, β is thermal expansion coefficient, a is effective thermal diffusivity of the porous medium, and μ and υ are viscosity and kinematic viscosity of the fluid, respectively. The symbols ε and ν denote the porosity of porous medium and fluid viscosity, respectively. In the present study, the heat capacity ratio o is taken to be unity, because the thermal properties of the solid matrix and the fluid are assumed identical (Bergman et al., 1986; Khanafer and Vafai, 2002). The momentum equation consists of the Brinkmann term, which describes viscous effects due to the presence of a solid body (Brinkmann, 1947). This form of the momentum equation is known as the Brinkmann-extended Darcy model. Lauriat and Prasad (1987) employed the Brinkmann-extended Darcy formulation to investigate

the buoyancy effects on natural convection in a vertical enclosure. Although the viscous boundary layer in the porous medium is very thin for most engineering applications, inclusion of this term is essential for heat-transfer calculations (Al-Amiri, 2000). However, the inertial effect was neglected as the natural convection flow was studied (Basak et al., 2006).

The variables are transformed into the dimensionless quantities, defined as,

$$X = \frac{x}{H}, \quad Y = \frac{y}{H}, \quad \tau = \frac{t\alpha}{H^2}, \quad U = \frac{uH}{\alpha}$$

$$V = \frac{vH}{\alpha}, \quad \varsigma = \frac{\omega H^2}{\alpha}, \quad \Psi = \frac{\psi}{\alpha}, \quad \theta = \frac{T - T_l}{T_h - T_l}$$
(10)

where ω and ψ represent dimensional vorticity and stream function, respectively, and the symbol α denotes thermal diffusivity. Temperatures T_l and T_h change their values according to the problem type. In the heating case, T_l is initial temperature of a medium and T_h is an ambient temperature. In the other case of cooling, T_h is set to be an initial temperature of the medium, while T_l is an ambient temperature instead. The governing equations are transformed into a vorticity-stream function formulation. Thus, the dimensionless form of the governing equations can be written as

$$\frac{\partial^2 \Psi}{\partial X^2} + \frac{\partial^2 \Psi}{\partial Y^2} = -\varsigma \tag{11}$$

$$\varepsilon \frac{\partial \varsigma}{\partial \tau} + U \frac{\partial \varsigma}{\partial X} + V \frac{\partial \varsigma}{\partial Y} = \varepsilon \Pr\left(\frac{\partial^2 \varsigma}{\partial X^2} + \frac{\partial^2 \varsigma}{\partial Y^2}\right) + \varepsilon^2 Ra \Pr\left(\frac{\partial \theta}{\partial X}\right) - \frac{\varepsilon^2 \Pr}{Da} \varsigma$$
 (12)

$$\sigma \frac{\partial \theta}{\partial \tau} + U \frac{\partial \theta}{\partial X} + V \frac{\partial \theta}{\partial Y} = \alpha \left(\frac{\partial^2 \theta}{\partial X^2} + \frac{\partial^2 \theta}{\partial Y^2} \right)$$
(13)

$$U = \frac{\partial \Psi}{\partial Y}, \quad V = -\frac{\partial \Psi}{\partial X}$$
 (14)

where the Darcy number, Da, is defined as κ/H^2 , and $\mathrm{Pr} = \nu/\alpha$ is the Prandtl number, where $\alpha = k_e/(\rho c_p)_f$ is the thermal diffusivity. The Rayleigh number Ra, which gives the relative magnitude of buoyancy and viscous forces, is defined as $\mathrm{Ra} = g\beta(T_i - T_\infty)\mathrm{H}^3/(\upsilon\alpha)$.

3. NUMERICAL PROCEDURE

The thermal properties of the porous medium are taken to be constant. Specific heat ratio of unity is assumed. The effective thermal conductivity of the porous medium considered is 10 W/m·K.

In the present study, the iterative finite difference method was used to solve the transient dimensionless governing equations [Eqs. (10)-(12)] subject to their corresponding initial and boundary conditions, given by Eqs. (1)-(4). Central-difference formulae were used for all spatial derivatives. The transient transport equations, Eqs. (12) and (13), were solved explicitly. A successive over-relaxation method (SOR) was utilized to solve for the flow kinematics relation given by Eq. (11). The velocity components, U and V, were computed according to Eq. (14). The approximation of convective terms is based on a second-order upwind finite differencing scheme, which correctly represents the directional influence of a disturbance. A uniform grid resolution of 61 × 61 was found to be sufficient for all smooth computations and computational time required in achieving steady-state conditions. Finer grids did not provide a noticeable change in the computed results.

3.1. Convective Cooling Boundary Condition

The finite difference form of boundary condition at the open part of the top surface was systematically derived based on the energy conservation principle. The boundary values of dimensionless temperature of a node i, j, and $\theta_{i,j}$ in the heating case are expressed as

$$\theta_{ij} = \frac{2\theta_{ij-1} + \theta_{i-1j} + \theta_{i+1j} + 2\frac{h\Delta y}{k}}{2\left(\frac{h}{k}\Delta Y + 2\right)}$$
(15)

where ΔY is the mesh size in y direction.

In the different case of cooling phenomenon, the expression is given by

$$\theta_{ij} = \frac{2\theta_{ij-1} + \theta_{i-1j} + \theta_{i+1j}}{2\left(\frac{h}{k}\Delta Y + 2\right)}$$
(16)

It can be noticed that both Eqs. (15) and (16) are independent of an ambient temperature T_{∞} , as it has been eliminated during the derivation. This feature is attractive since the solutions can be obtained regardless of a value of T_{∞} .

3.2. Corrected Formulation of Nusselt Number

The local Nusselt number (Nu) at the cooled horizontal surface is used as a tool to determine the ratio of convection heat transfer to conduction heat transfer within the porous enclosure. The accurate derivation of Nu is extremely important from the standpoint of determining the rate of heat transfer occurring at a surface. Based on the concept of energy balance at the surface for the cooling case,

$$-k \left. \frac{dT}{dy} \right|_{y=H} = h(T_{\rm H} - T_{\infty}) \tag{17}$$

where H is indicated in Fig. 1 and with the definition of Nu,

$$Nu = \frac{hH}{k} = -\frac{H}{(T_H - T_\infty)} \left. \frac{dT}{dy} \right|_{Y=H}$$
 (18)

In terms of the dimensionless quantities θ and Y defined in the preceding Eq. (10), Nu will take the form

$$Nu = -\frac{1}{\theta_H} \left. \frac{d\theta}{dY} \right|_{Y=1} \tag{19}$$

where θ_H is the dimensionless temperature at the top surface.

The new formulation of Nu in the present work has not yet been found in the literature. This modified form of Nu takes into account temperature variation at the cooled surface. The average Nusselt number, $\overline{\text{Nu}}$, is computed according to

$$\overline{\mathrm{Nu}} = \int_{1}^{\mathrm{W-L}} \frac{\mathrm{Nu}(x)dx}{l} \tag{20}$$

where l is the length of the gap at the top wall.

In order to verify the accuracy of the present numerical study, the results obtained by the present numerical model were validated against the Benchmark solutions for natural convection in a cubic cavity (Wakashima and Saitoh, 2004). The comparisons tabulated in Table 1 reveal an excellent agreement within 1.5% difference. The present computed results were compared with those obtained by Aydin (2000) for free convection flow in a cavity, with a side-heated isothermal wall, filled with pure air (Pr = 0.7) for a Rayleigh number of 104. It was found that the solutions have good agreement with the previously published work. The results of selected tests are given in Table 2, which shows good agreement with the maximum value of the stream function and the maximum values of the horizontal and vertical velocity components between the present solution and that of Aydin. Moreover, the results from the present numerical model were compared with the solution of Nithiarasu et al. (1997) in the presence of porous medium for an additional source of confidence, as shown in Fig. 2 for streamlines and isotherms for which the compared contours have the same range of contour levels. The values $Ra = 10^4$, Da = 0.01, and $\varepsilon = 0.6$ were chosen. Table 3 clearly shows good agreement of the maximum values of the stream function and the vertical velocity component between the present solution and that of Nithiarasu et al (1997). All of these favorable comparisons lend confidence to the accuracy of the present numerical model.

Table 1

Comparison of the results obtained in the present study with those of the benchmark solutions for natural convection of air (Wakashima and Saitoh, 2004)

Ra	ω_{center}	Difference (%)	(%)	Difference	V _{max} (%)	Difference
10 ⁴ Present Previous work	1.111 1.102	0.82	0.202 0.199	1.51	0.220 0.222	0.2
10 ⁵ Present Previous work	0.262 0.258	1.55	0.144 0.142	1.41	0.249 0.246	1.22

Table 2

Comparison of the results obtained in the present study with those of Aydin (2000)

	Present work	Published work	Difference (%)
$\psi_{\rm max}$	5.070	5.087	0.33
$U_{\rm max}$	16.300	16.225	0.46
$V_{\rm max}$	19.730	19.645	0.43

Table 3

Comparison of the results obtained in the present study with those of Nithiarasu et al. (1997). (Da = 0.01, Ra = 10^4 , porosity = 0.6)

	Present work	Published work	Difference (%)
ψ_{max}	2.53	2.56	1.17
$V_{\rm max}$	9.49	9.34	1.60

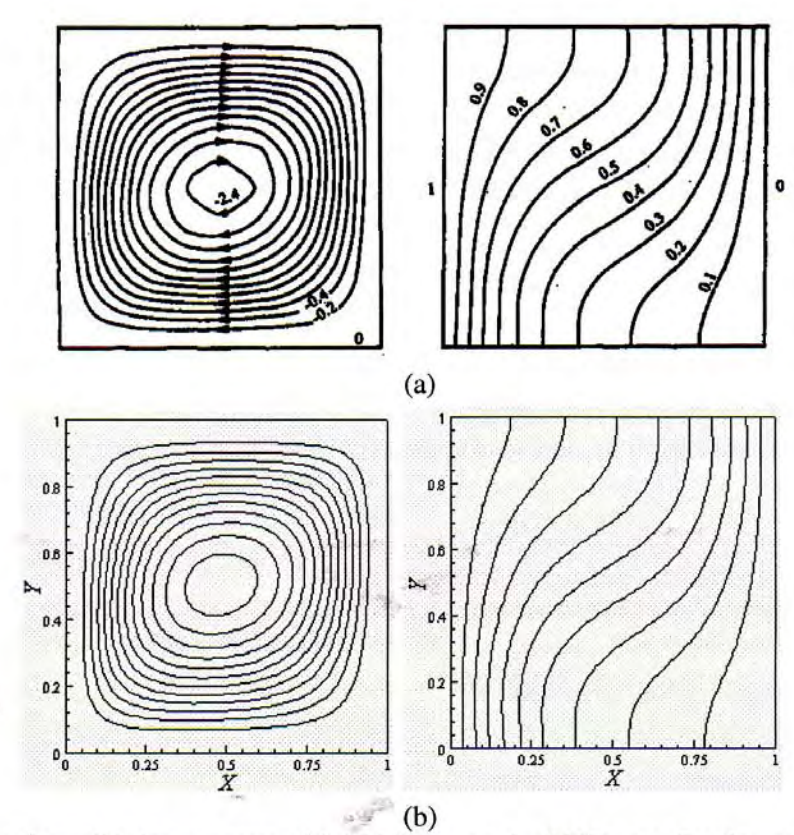


Figure 2. Test results for validation purposes: (a) Nithiarasu et al. (1997): non-Darcian model (including inertial and boundary effect), and (b) present simulation: Brinkman-extended Darcy model, which accounts for viscous effects

包

4. RESULTS AND DISCUSSION

The following discussions include the numerical results from the present study, which focuses on transient flow and thermal behaviors. Initial values of θ for an entire domain are set to 1 based on Eq. (10), as the ambient temperature is lower than the medium temperature in the cavity. The investigations were conducted for a range of controlling parameters, which are Darcy number (Da), Rayleigh number (Ra), and the convective heat-transfer coefficient (h). The uniform porosity ε of 0.8 and unity aspect ratio (A = 1) were considered throughout in the present study. In order to assess the global effects of these parameters, the streamlines and isotherm distributions inside the entire cavity are presented. All the figures have the same range of contour levels to facilitate direct comparisons.

The resulting computational fields were extracted at the time adequately long to ensure sufficient energy transferred throughout the domain. Figure 3 displays instantaneous images of the contour plots during the thermal and flow evolution. A Rayleigh number of 5×10^4 , Da = 0.1, Pr = 1.0, $h = 60 \text{ W/m}^2\text{K}$, and $\varepsilon = 0.8$ are considered. The two columns represent contours of temperature and stream function, respectively, from left to right. With the same contour levels, comparisons can be made directly. The four snapshots from top to bottom in each column are results taken at the dimensionless times $\tau = 0.013$, 0.088, 0.168, and 0.245. The vertical temperature stratification is observed. The streamline contours exhibit circulation patterns which are characterized by the two symmetrical vortices. The fluid flows as it is driven by the effect of buoyancy. This effect is distributed from the top wall of the cavity where the fluid is cooled through the partially open surface, causing lower temperature near the top boundary. The existence of the nonuniform temperature along the top surface and a decrease of density in the direction of gravitational force lead to an unstable condition. Thus, the buoyancy effect is associated with the lateral temperature

gradients at locations near the top surface. Hightemperature portions of fluid become lighter than the lower temperature portions at the middle where the wall is open. These light portions from two sides then expand laterally toward the center, compressing the lower temperature portions, which are heavier. As a result, the downward flows along the vertical centerline originate, while the lighter fluid rises, cooling as it moves. Consequently, the circulation flow pattern is generated. The clockwise and counter-clockwise circulations are located on the left side and right side, respectively, within the enclosure. The circulations get larger and expand downward with time. An increase in strength of the vortices develops fast during early simulation times, and its maximum magnitude reaches 6.0. Subsequently, the vortices are weakened. Similarly, temperature distribution progressively evolves relatively fast in the early times. Slow evolution is observed after that. This result corresponds well with the decrease in strength of flow circulations.

The resulting computational fields of the heating scenario are demonstrated in Fig. 4. For purposes of comparison, the parameter set remains unchanged. Similarly, the two columns represent temperature and stream function taken at the dimensionless times $\tau = 0.013$, 0.088, and 0.168. The vertical temperature stratification is observed. The streamline contours exhibit circulation patterns which are characterized by the two symmetrical vortices. The fluid flows as it is driven by the effect of buoyancy. This effect is distributed from the top wall of the cavity where the fluid is heated through the partially open area. Unlike the cooling case in which a presence of negative density mainly causes an unstable condition, in the heating case the lateral density gradient near the top surface is the only cause to the unstable condition that actually leads to the buoyancy force. This explains why the heated circulations are weaker than the cooled circulations presented earlier. Heated portions of the fluid become lighter than the rest of the fluid and are expanded laterally away from the center to the sides, then flow down along the two vertical walls, leading

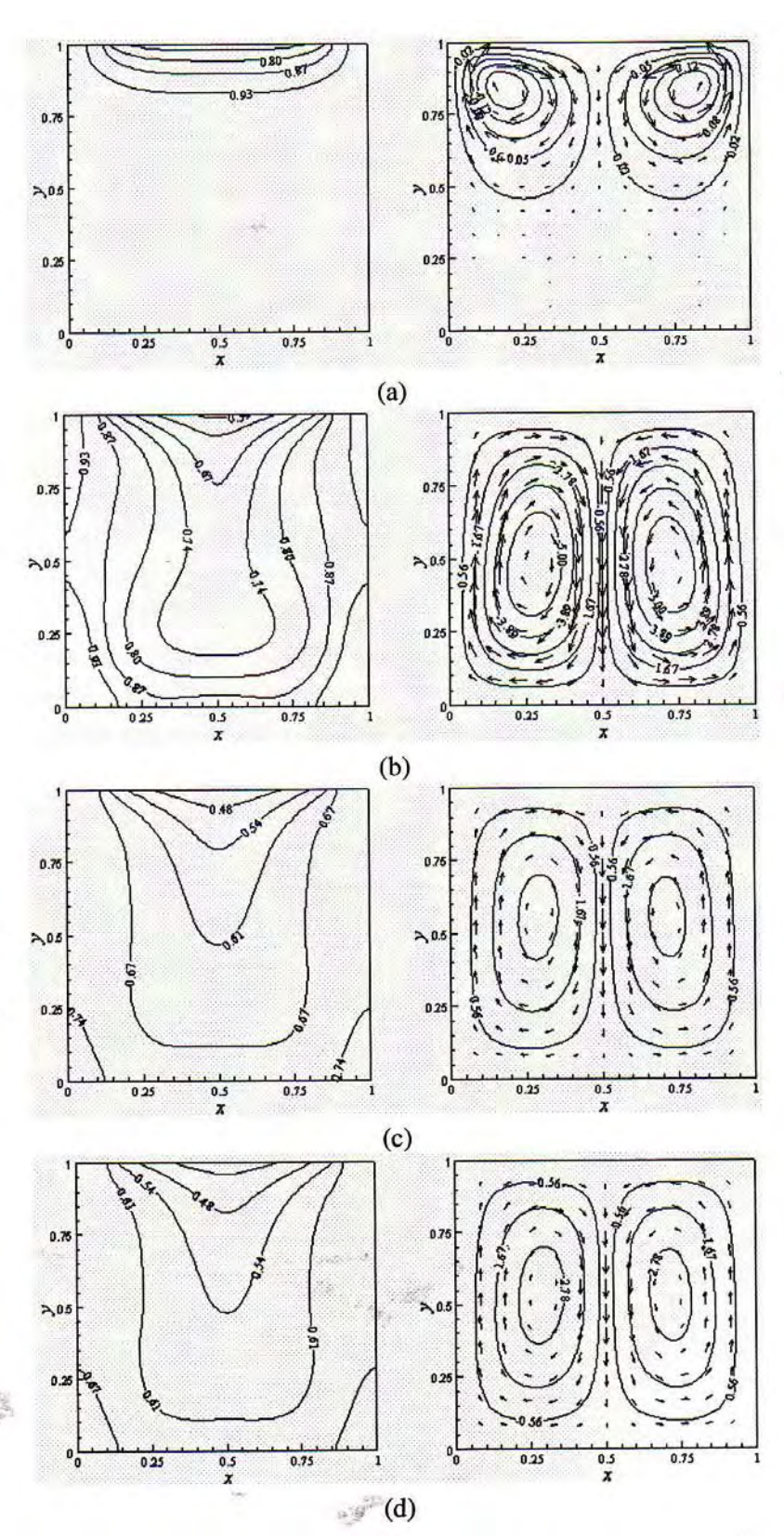


Figure 3. Sequential files with the cooling boundary for contours of temperature and streamlines at times τ = (a) 0.013, (b) 0.088, (c) 0.168, and (d) 0.245. (Ra = 5×10^4 , Da = 0.1, Pr = 1.0, ε = 0.8, and h = 60 W/m²K)

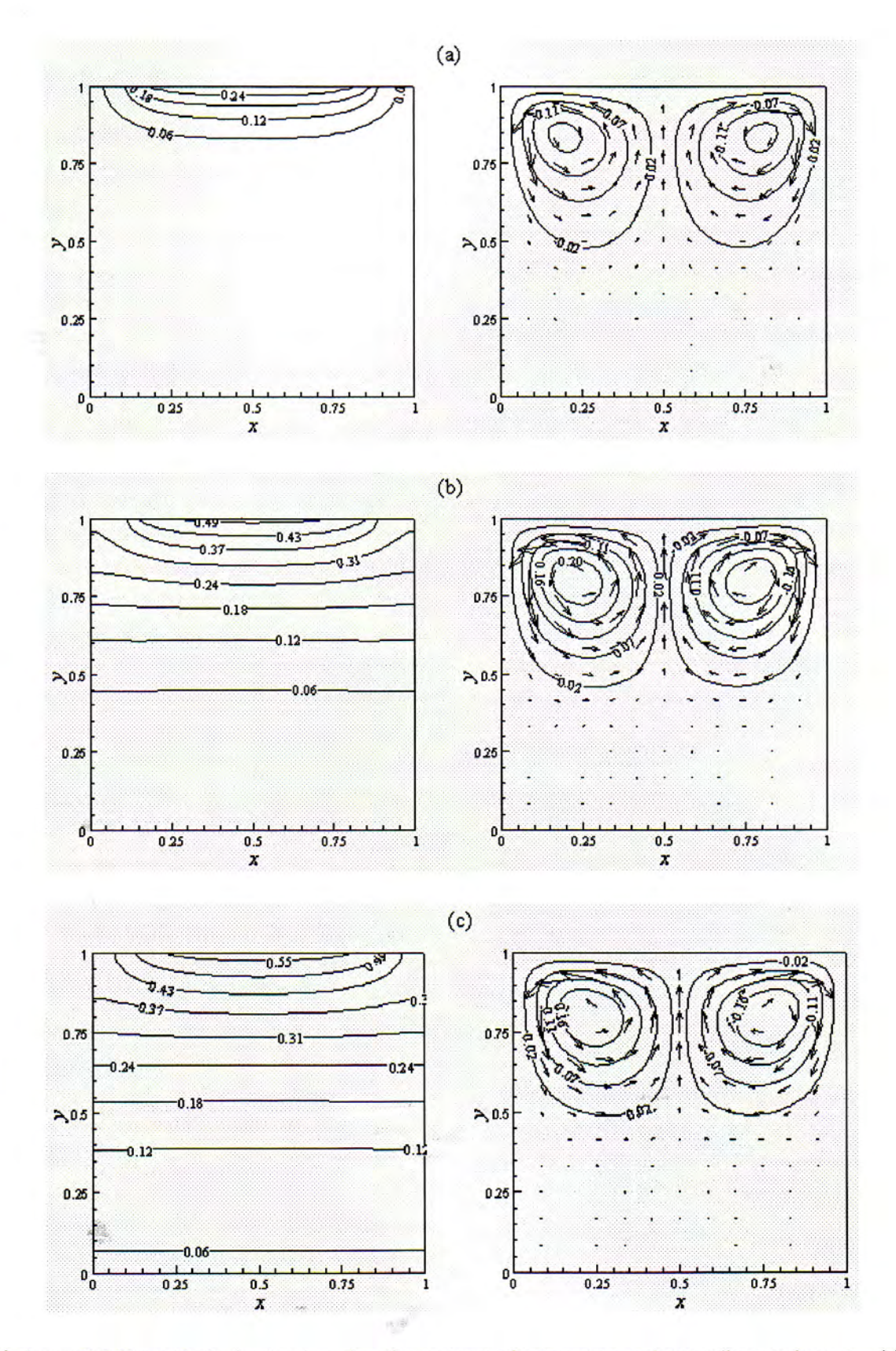


Figure 4. Sequential files with the heating boundary for contours of temperature and streamlines at times τ = (a) 0.013, (b) 0.088, and (c) 0.168. (Ra = 5×10^4 , Da = 0.1, Pr = 1.0, ϵ = 0.8, and h = 60 W/m²K)

to the counter-clockwise and clockwise flow circulations. These results suggest that the buoyancy forces are able to overcome the retarding influence of viscous forces. Note that directions of circulations are opposite to those under cooling condition. An increase in strength of the vortices develops fast during early simulation times and its maximum magnitude reaches 0.25, which is considerably small. Therefore, profiles of temperature contours look similar to those for a stationary fluid, in which the heat transfer is caused by conduction. Similarly, temperature distribution progressively evolves relatively fast in the early times. This result corresponds to the decrease in strength of flow circulations. In the remaining area, the fluid is nearly stagnant, suggesting that conduction is dominant due to minimal flow activities. This is because of prevailing viscous effects. It is evident from Figs. 3 and 4 that the cooling case provides a considerably faster thermal evolution and thereby greater convection rate. Furthermore, heat transfer in the vertical direction is much greater than that in the spanwise direction. The reader is directed to Pakdee and Rattanadecho (2006) for more detailed discussions of heating configuration.

Figure 5 shows the roles of Rayleigh number on the heat-transfer mechanism. The computed data was extracted at $\tau = 0.155$. Various Rayleigh numbers $(Ra = 5 \times 10^3, 10^4, 5 \times 10^4 \text{ and } 10^5)$ are examined, whereas the Darcy number of 0.1, porosity of 0.8, and h of 60 W/m2 K are fixed. The Rayleigh number provides the ratio of buoyancy forces to change in viscous forces. As Rayleigh number increases, the buoyancy-driven circulations inside the enclosure become stronger, as seen from greater magnitudes of stream function. For large Ra (Ra = 5×10^4 and 10^5), contour lines of temperature penetrate faster relative to the low-Ra case, especially near the central locations. The result is more pronounced for larger Ra. This incident results from strong flow in the downward direction around the central domain. The downward flows assist heat to transfer toward the bottom of the enclosure. In contrast, near the vertical walls

where the upward flows are present, the thermal propagation is hindered.

Effects of the Darcy number on the fluid flow and temperature inside the rectangular cavity are depicted in Fig. 6. The contour of isotherms and streamlines at $\tau = 0.155$ are plotted for different Darcy numbers, while ε , Pr, and h are kept at 0.8, 1.0, and 60 W/m²K, respectively. Relatively high Ra of 5 x 104 is chosen. The Darcy number, which is directly proportional to the permeability of the porous medium, was set to 0.0001, 0.001, and 0.1. The case in which the porous medium is absent corresponds to an infinite Darcy number. The presence of a porous medium within the rectangular enclosure results in a force opposite the flow direction which tends to resist the flow, which corresponds to suppression in the thermal currents of the flow as compared to a medium with no pores (infinite Darcy number). It is evident that the increase in Da enhances the streamline intensities, thereby assisting downward flow penetration, which causes the streamline lines, i.e., two symmetrical vortices to stretch further away from the top surface. This results in expanding the region for which the convection significantly influences an overall heat-transfer process. Furthermore, the evolution results reveal a faster rate of vertical temperature distribution than the lateral rate. The results are consistent with the thermal behaviors observed in Fig. 5 for the same reasoning, which confirms how a flow direction impacts the convection heat transfer. However, as the Darcy number decreases, the flow circulations as well as thermal penetration are progressively retarded due to the reduced permeability of the medium. Figure 6(d) (Da = 0.0001) indicates that as the Darcy number approaches zero, the two circulations confined within the top domain appear very weak. In the remaining area the fluid is nearly stagnant with a very small temperature gradient, suggesting that conduction is dominant due to minimal flow activities.

Figure 7 presents how the average Nusselt number changes with time for a variety of Rayleigh numbers. The local Nu at the open portion on the top boundary

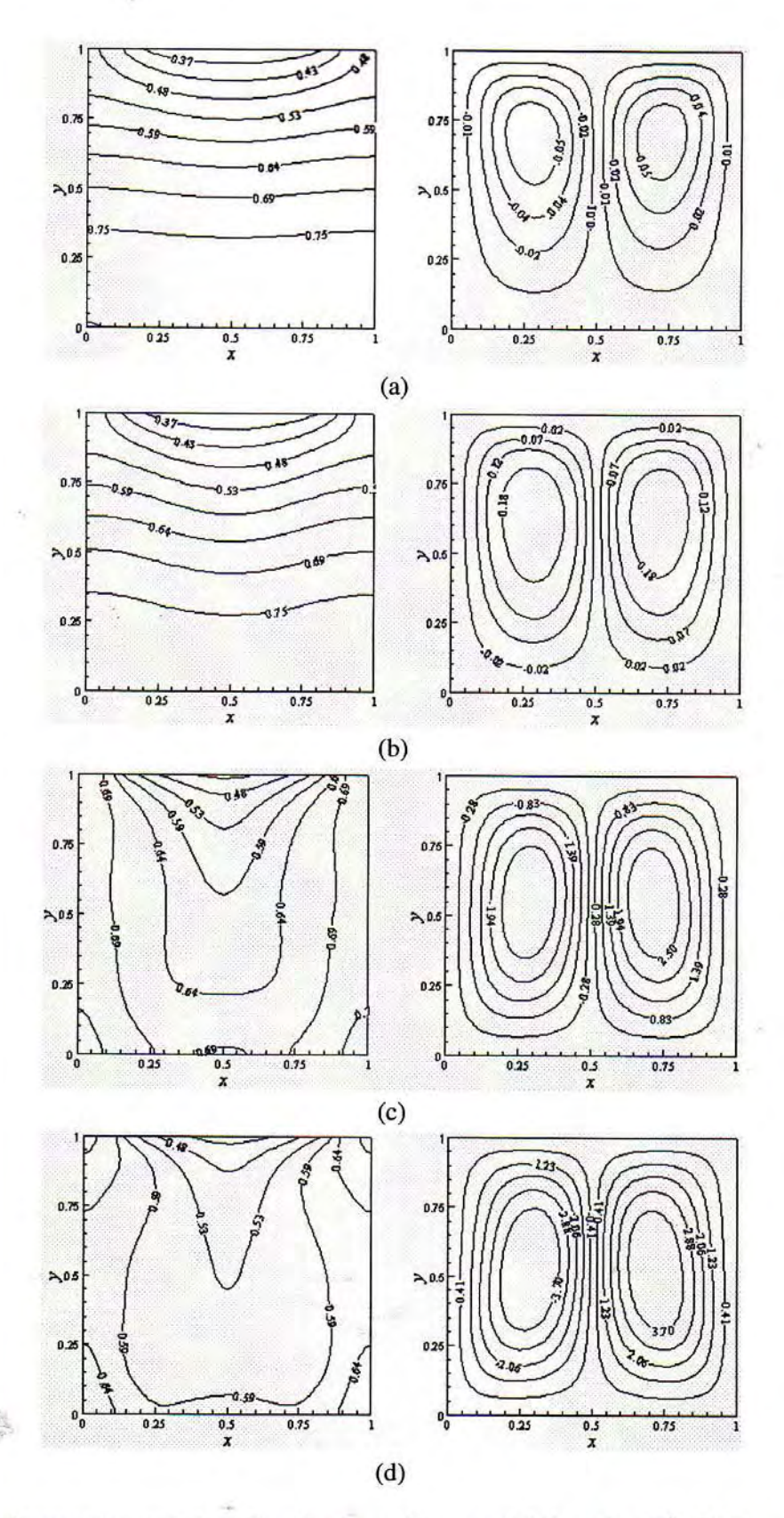


Figure 5. Contours of temperature and streamlines for the cooling case: (a) $Ra = 5 \times 10^3$, (b) $Ra = 10^4$, (c) $Ra = 5 \times 10^4$, and (d) $Ra = 10^5$. (Da = 0.1, h = 60 W/m²K, Pr = 1.0, and $\epsilon = 0.8$)

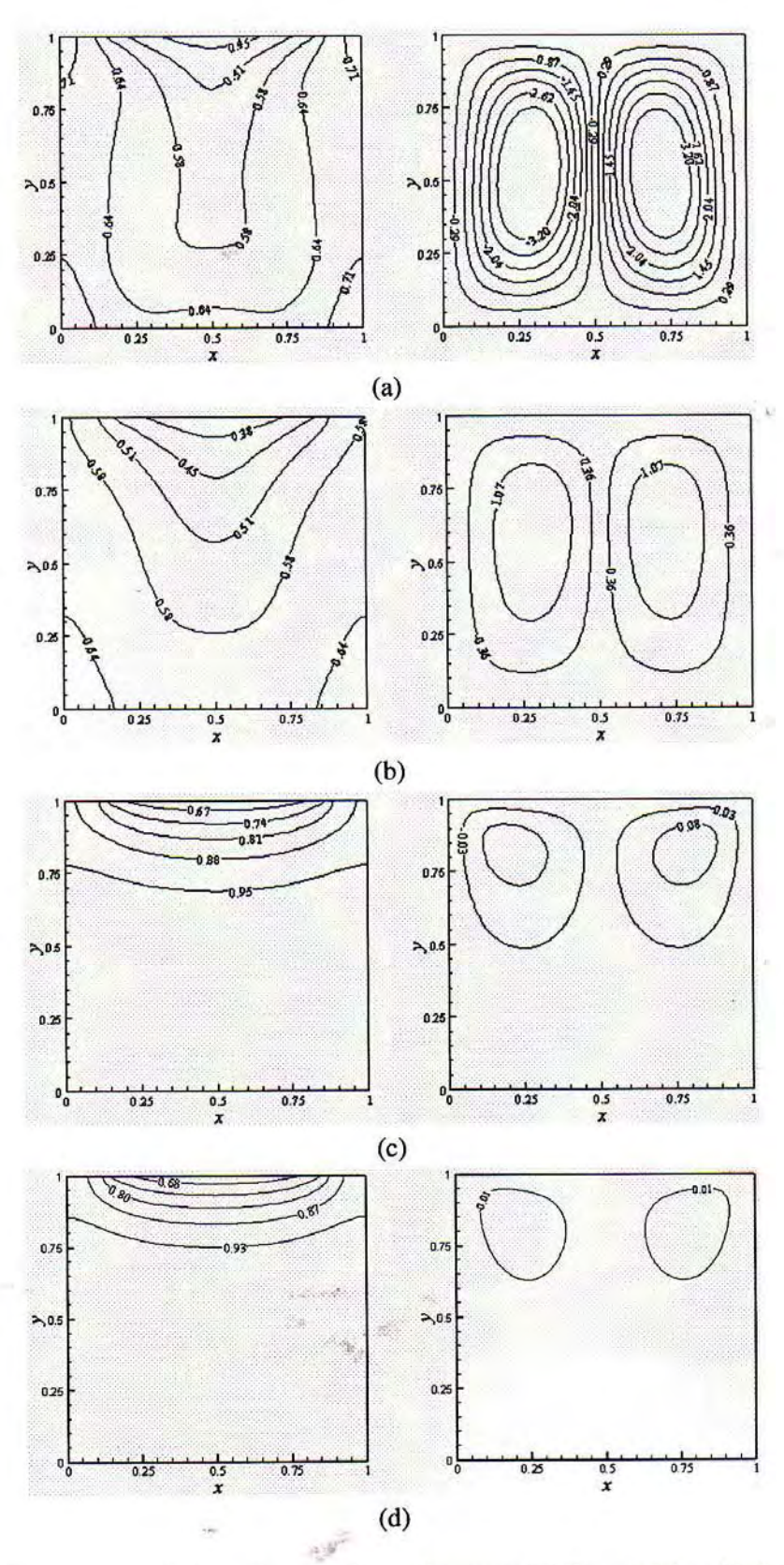


Figure 6. Contours of temperature and streamlines for the cooling case: (a) Da = infinity, (b) Da = 0.01, (c) Da = 0.001, and (d) Da = 0.0001. (Ra = 5×10^4 , h = 60 W/m²K, Pr = 1.0, and ε = 0.8)

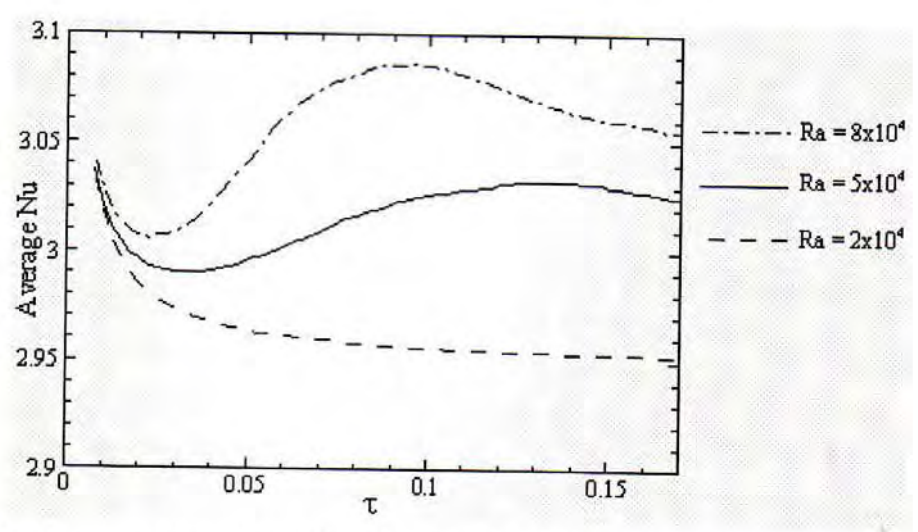


Figure 7. Variations of the average Nusselt number with time for different Rayleigh numbers. (Da = 0.01, h = 60 W/m²K, Pr = 1.0, and ε = 0.8)

is computed according to Eq. (19). The average Nusselt number \overline{Nu} is then obtained based on Eq. (20). Initially, the value of $\overline{\mathrm{Nu}}$ decreases rapidly for all Rayleigh number values, clearly due to the fast reduction of temperature gradients. In the case of a low Rayleigh number of 2×10^4 , $\overline{\text{Nu}}$ progressively decreases with time, while for higher Ra $(5 \times 10^4$, 8×10^4), $\overline{\mathrm{Nu}}$ values become greater and reach peak values after some time. By further increasing Ra (8×10^4) , a higher maximum Nu is reached more quickly due to greater flow intensities. At late simulation times when a stable state is approached, the values of Nu continually decrease and essentially level off at late times, thereby diminishing heat transfer by means of heat convection. It can be expected that $\overline{\mbox{Nu}}$ will continue to decrease with time as the steady state is reached.

To gain insight into the observation made, the local values of the corresponding thermal and flow behaviors were traced for Ra of 8×10^4 . The data are extracted and depicted in Fig. 8 at τ of 0.02, 0.1, and 0.16. The streamlines and isotherms are illustrated in Figs. 8a–c at $\tau=0.02$, 0.1, and 0.16, respectively. At $\tau=0.02$, the averaged Nu is small due to minimal flow activities. Then $\overline{\text{Nu}}$ gets higher as the flows gets stronger, which can be seen in Fig. 8b at $\tau=0.1$. The effect of the rigorous flows overcomes the continual reduction of temperature gradient, resulting in the

increase in $\overline{\text{Nu}}$. At the subsequent times, the viscous effect increasingly weakens the flows as shown in Fig. 8c. As a result, the reduction of temperature gradient prevails, causing $\overline{\text{Nu}}$ to decrease. These results correspond well with the variation of the averaged Nu with time, depicted in Fig. 7. The results confirm the validation of the proposed formulation of Nu.

To better understand the effects of Darcy number on the heat-transfer behavior, variations of $\overline{\text{Nu}}$ with time for different Darcy number are shown in Fig. 9. The resulting plots show interesting evidence of similar variations of $\overline{\text{Nu}}$ on Da and those on Ra, which was observed previously in Fig. 7 Average Nu correlates with Ra in a way similar to correlation of Nu with Da. Further increasing values of Da (0.05 and 0.1) cause larger $\overline{\text{Nu}}$ variations. Locations of the peak values are altered relative to Da value. A peak of profile is reached more quickly for higher Da. Greater Da gives higher $\overline{\text{Nu}}$, suggesting that the higher overall heat-transfer rate is due to more energetic vortices. However, $\overline{\text{Nu}}$ substantially reduces at late times.

5. CONCLUSIONS

Numerical simulations of natural convection flow through a fluid-saturated porous medium in a rectangular cavity due to cooling convection at the top surface were performed. Transient effects of asso-

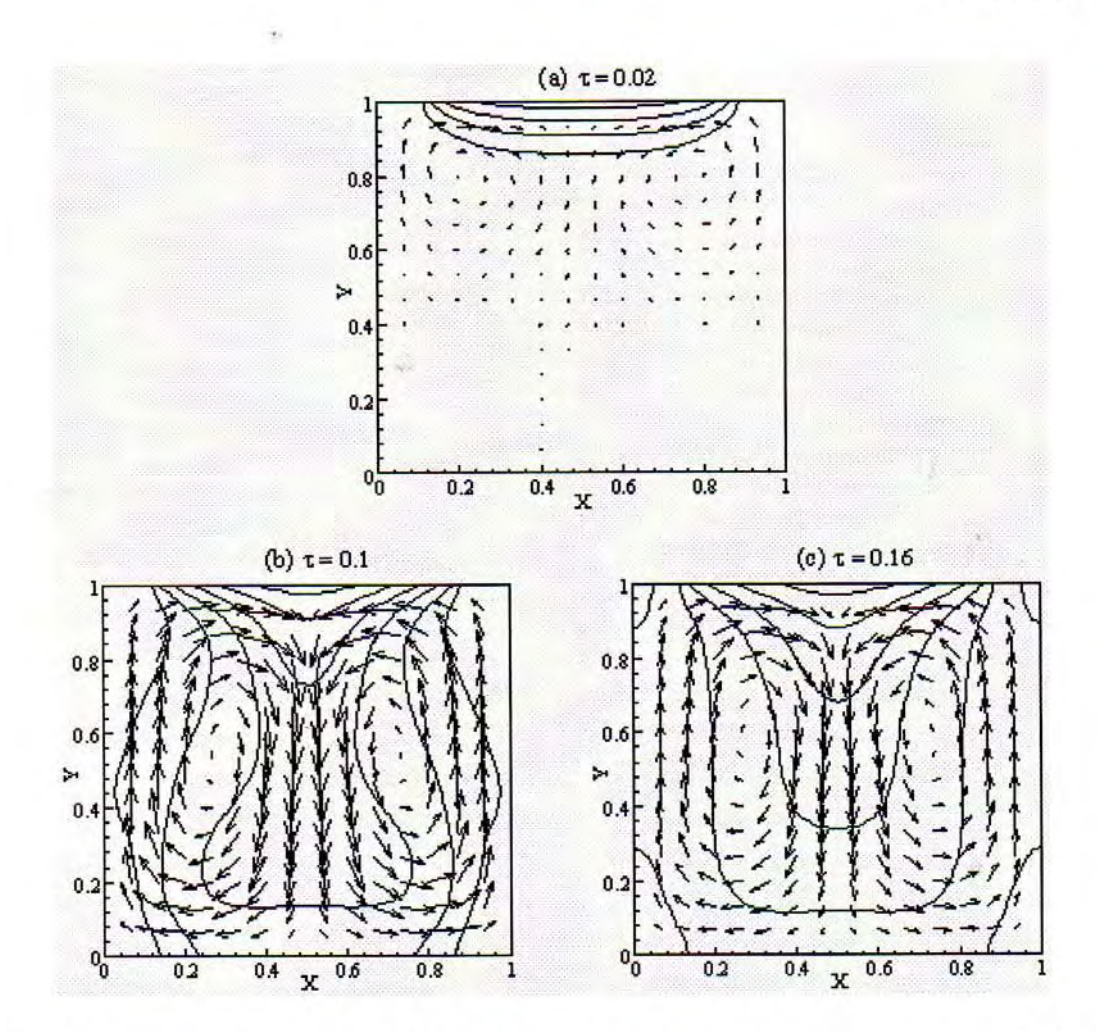


Figure 8. (a)–(c) Temperature contours overlaid by velocity vectors at $\tau=0.02,\,0.1,\,$ and 0.16, respectively. Data is taken from that of Fig. 7 for Ra = 8×10^4

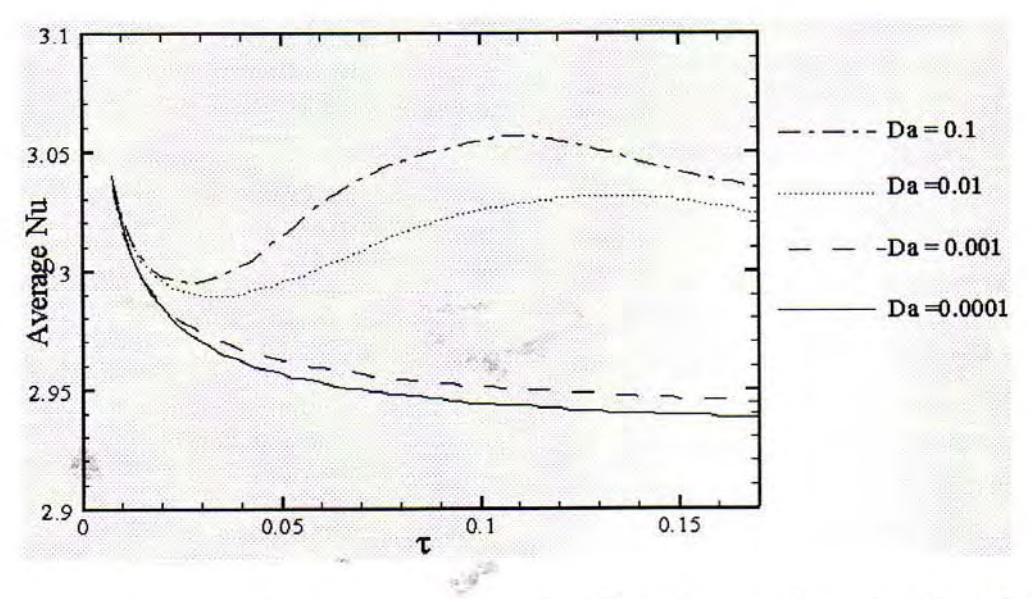


Figure 9. Variations of the average Nusselt number with time for different Darcy numbers. (Ra = 5×10^4 , h = $60 \text{ W/m}^2\text{K}$, Pr = 1.0, and $\varepsilon = 0.8$)

ciated controlling parameters were examined. The two-dimensional flow is characterized mainly by two symmetrical eddies that are initiated by the buoyancy effect. In the cooling case, the buoyancy effect is associated not only with the lateral temperature gradient at locations near the top surface, but also with the condition that the density gradient is negative in the direction of gravitational force. The buoyancy force is induced solely by the lateral temperature gradient in the heating case. The cooling and heating flow directions are opposite. Cooling flows are much stronger due to greater buoyancy effects, indicating higher overall convection rate. The heat-transfer mechanism is analyzed using the newly derived formulation of Nu. Heat-transfer rate is faster around a vertical symmetric line relative to the near-wall regions. Large Ra numbers increase streamline intensities, thus enhancing the downward flow penetration. The temperature stratification penetrates deeper toward the bottom wall and temperature range within the domain is extended. Therefore it enlarges the region where convection mode is significant. Small Darcy number values hinder the flow circulations. Therefore, heat transfer by convection is considerably suppressed. Furthermore, the new formulation of Nu captures the heat-transfer behaviors reasonably correctly. Interestingly, the dependences of Nu on Da and on Ra are found to have the same trends.

ACKNOWLEDGMENTS

This research was supported by the Thailand Research Fund (TRF) 2008 under contract no. MRG5180238.

REFERENCES

- Al-Amiri, A. M., Analysis of Momentum and Energy Transfer in a Lid-Driven Cavity Filled with a Porous Medium, *Int. J. Heat Mass Transfer*, vol. 43, pp. 3513–3527, 2000.
- Al-Amiri, A. M., Natural Convection in Porous Enclosures: The Application of the Two-Energy Equa-

- tion Model, Numer. Heat Transfer, Part A, vol. 41, pp. 817–834, 2002.
- Aydin, O., Determination of Optimum Air-Layer Thickness in Double-Pane Windows, *Energy Build.*, vol. 32, pp. 303–308, 2000.
- Basak, T., Roy, S., Paul, T., and Pop, I., Natural Convection in a Square Cavity Filled with Porous Medium: Effects of Various Thermal Boundary Conditions, Int. J. Heat Mass Transfer, vol. 49, pp. 1430–1441, 2006.
- Beckermann, C., Viskanta, R., and Ramadhyani, S., A Numerical Study of Non-Darcian Natural Convection in a Vertical Enclosure Filled with a Porous Medium, Numer. Heat Transfer, vol. 10, pp. 557–570, 1986.
- Bera, P., Eswaran, V., and Singh, P., Numerical Study of Heat and Mass Transfer in an Anisotropic Porous Enclosure Due to Constant Heating and Cooling, *Numer*. *Heat Transfer Part A*, vol. **34**, pp. 887–905, 1998.
- Bera, P., and Khalili, A., Double-Diffusive Natural Convection in an Anisotropic Porous Cavity with Opposing Buoyancy Forces: Multi-Solutions and Oscillations, Int. J. Heat Mass Transfer, vol. 45, pp. 3205–3217, 2002.
- Bergman, T. L., Incropera, F. P., and Viskanta, R., Correlation of Mixed Layer Growth in Double-Diffusive, Salt-Stratified System Heated from Below, J. Heat Transfer, vol. 108, pp. 206–211, 1986.
- Bilgen, E., and Mbaye, M., Be'nard Cells in Fluid-Saturated Porous Enclosures with Lateral Cooling, *Int. J. Heat Fluid Flow*, vol. **22**, pp. 561–570, 2001.
- Brinkmann, H. C., On the Permeability of Media Consisting of Closely Packed Porous Particles, Appl. Sci. Res., vol. 1, pp. 81–86, 1947.
- Bradean, R., Ingham, D. B., Heggs, P. J., and Pop, I., The Unsteady Penetration of Free Convection Flows Caused by Heating and Cooling Flat Surfaces in Porous Media, *Int. J. Heat Mass Transfer*, vol. 40, pp. 665–687, 1997.
- Cheng, P., Heat Transfer in Geothermal Systems, Adv. Heat Transfer, vol. 4, pp. 1–105, 1978.
- Desai, C. P., Vafai, K., and Keyhani, M., On the Natural-Convection in a Cavity with a Cooled Top Wall and Multiple Protruding Heaters, *J. Electron. Packag.*, vol. 117, pp. 34–45, 1995.
- El-Refaee, M. M., Elsayed, M. M., Al-Najem, N. M., and Noor, A. A., Natural Convection in Partially Cooled Tilted Cavities, Int. J. Numer. Methods, vol. 28, pp. 477–499, 1998.

- Imberger, J., and Hamblin, P. F., Dynamics of Lakes, Reservoirs, and Cooling Ponds, Ann. Rev. Fluid Mechanics, vol. 14, pp. 153–187, 1982.
- Khanafer, K. M., and Chamkha, A. J., Mixed Convection Flow in a Lid-Driven Enclosure Filled with a Fluid-Saturated Porous Medium, *Int. J. Heat Mass Transfer*, vol. 42, pp. 2465–2481, 1998.
- Khanafer, K., and Vafai, K., Double-Diffusive Mixed Convection in a Lid-Driven Enclosure Filled with a Fluid-Saturated Porous Medium, Numer. Heat Transfer, Part A, vol. 42, pp. 465–486, 2002.
- Kim, S. J., Kim, D., and Lee, D. Y., On the Local Thermal Equilibrium in Microchannel Heat Sinks, *Int. J. Heat Mass Transfer*, vol. 43, pp. 1735–1748, 2000.
- Lauriat, G., and Prasad, V., Natural Convection in a Vertical Porous Cavity: A Numerical Study for Brinkmann-Extended Darcy Formulation, ASME J. Heat Transfer, vol. 109, pp. 295–320, 1987.
- Lauriat, G., and Prasad, V., Non-Darcian Effects on Natural Convection in a Vertical Porous Enclosure, *Int. J. Heat Mass Transfer*, vol. **32**, pp. 2135–2148, 1989.
- Marafie, A., and Vafai, K., Analysis of Non-Darcian Effects on Temperature Differentials in Porous Media, Int. J. Heat Mass Transfer, vol. 44, pp. 4401–4411, 2001.
- Mohammad, A. A., Nonequilibrium Natural Convection in a Differentially Heated Cavity Filled with a Saturated Porous Matrix, J. Heat Transfer, vol. 122, pp. 380– 384, 2000.
- Nield, D. A., and Bejan, A., Convection in Porous Media, New York: Springer, 1999.
- Nithiarasu, P., Seetharamu, K. N., and Sundararajan, T., Natural Convective Heat Transfer in a Fluid Saturated Variable Porosity Medium, Int. J. Heat Mass Transfer, vol. 40, pp. 3955–3967, 1997.
- Nithiarasu, P., Seetharamu, K. N., and Sundararajan, T., Numerical Investigation of Buoyancy Driven Flow in a Fluid Saturated Non-Darcian Porous Medium, *Int. J.*

- Heat Mass Transfer, vol. 42, pp. 1205-1215, 1998.
- Oosthuizen, P. H., and Patrick, H., Natural Convection in an Inclined Square Enclosure Partly Filled with a Porous Medium and with a Partially Heated Wall, American Society Mechanical Engineers, Heat Transfer Division, HTD 302, pp. 29–42, 1995.
- Oztop, H. F., Natural Convection in Partially Cooled and Inclined Porous Rectangular Enclosure, *Int. J. Thermal Sci.*, vol. **46**, pp. 149–156, 2007.
- Pakdee, W., and Rattanadecho, P., Unsteady Effects on Natural Convective Heat Transfer through Porous Media in Cavity Due to Top Surface Partial Convection, Appl. Thermal Eng., vol. 26, pp. 2316–2326, 2006.
- Pop, I., and Ingham, D. B., Convective Heat Transfer, Mathematical and Computational Modeling of Viscous Fluids and Porous Media, Oxford: Pergamon, 2001.
- Ratanadecho, P., Aoki, K., and Akahori, M., A Numerical and Experimental Investigation of the Modeling of Microwave Drying Using a Rectangular Wave Guide, J. Drying Technol., vol. 19, pp. 2209–2234, 2001.
- Ratanadecho, P., Aoki, K., and Akahori, M., Influence of Irradiation Time, Particle Sizes and Initial Moisture Content During Microwave Drying of Multi-Layered Capillary Porous Materials, ASME J. Heat Transfer, vol. 124, pp. 151–161.
- Wakashima, S., and Saitoh, T. S., Benchmark Solutions for Natural Convection in a Cubic Cavity Using the High-Order Time-Space Method, *Int. J. Heat Mass Transfer*, vol. 47, pp. 853-864, 2004.
- Stanish, M. A., Schager, G. S., and Kayihan, F., A Mathematical Model of Drying for Hygroscopic Porous Media, AIChE J., vol. 32, pp. 1301-1311, 1986.
- Tong, T. W., and Subramanian, E., A Boundary-Layer Analysis for Natural Convection in Vertical Porous Enclosures, Use of the Brinkman-Extended Darcy Model, ASME J. Heat Transfer, vol. 28, pp. 563–571, 1985.
- Vafai, K., Handbook of Porous Media, New York: Marcel Dekker, 2000.

Submitted Manuscript

Journals Publications Page 1 of 1



<< Back Withdraw Printer Friendly

Released for production

Publication Issue Paper published

Proof of final paper provided

Author approved proof of final paper

Home | Paper Status | Submit Paper | Author Resources | Technical Journals | Contact | Help

This site works best with: Internet Explorer 6.0+ • Firefox 2.0+ • Netscape 7.0+ • Acrobat Reader 5.0+

Natural Convection in a Saturated Variable-Porosity Medium due to Microwave

Heating

Watit Pakdee¹ and Phadungsak Rattanadecho

Authors' Research Center of Microwave Utilization in Engineering (R.C.M.E.)

Department of Mechanical Engineering, Thammasat University, Rangsit

Campus Klong Luang, Pathumthani, Thailand

Abstract

The microwave heating of a porous medium with a non-uniform porosity is numerically

investigated, based on the proposed numerical model. A two-dimensional variation of porosity of

the medium is considered. The generalized non-Darcian model developed takes into account of

the presence of a solid drag and the inertial effect. The transient Maxwell's equations are solved

by using the finite difference time domain (FDTD) method to describe the electromagnetic field

in the wave guide and medium. The temperature profile and velocity field within a medium are

determined by the solution of the momentum, energy and Maxwell's equations. The coupled

non-linear set of these equations are solved using the SIMPLE algorithm. In this work, a detailed

parametric study is conducted for a heat transport inside a rectangular enclosure filled with

saturated porous medium of constant or variable porosity. The numerical results agree well with

the experimental data. Variations in porosity significantly affect the microwave heating process

as well as convective flow pattern driven by microwave energy.

Keywords: Microwave heating, Non-uniform porosity, Natural convection, Saturated

porous media, Rectangular wave guide

Author to whom correspondence should be addressed; E-mail address: pwatit@engr.tu.ac.th, and wpele95@yahoo.com Tel: 011 662 5643001-5, Fax: 011 662 5643010

1. INTRODUCTION

Microwave heating of a porous medium are widely implemented in industries such as heating food, ceramic, biomaterial, concrete etc. Since microwave energy has many advantages such as short time process, high thermal efficiency, friendly with environment and high product quality. Microwave radiation penetrates into a material and heats the material by a dipolar polarization that occurs millions times of each second. A number of previous works focused on drying of unsaturated porous media in which heat and mass transfers were modelled [1-6].

Nevertheless, most of the studies dealt with solid materials and focused on conduction heat transfer within a medium. Some works studied a natural convection induced by microwave heating of fluid, since a complex distribution of electromagnetic wave is shown to be a complicate effect on flow field [7-11]. Effects of natural convection and dielectric properties on liquid layers were studied numerically and experimentally. The heating kinetics strongly depends on dielectric properties [7]. Natural convection due to buoyancy force strongly affects flow pattern within water layer during microwave heating process, and clearly enhances temperature distribution in the layer [8]. Recently, Cha-um et al. [8] experimentally investigated the heating process within a packed bed filled with glass beads and water and found that a location of sample relative to that of heat source has an important effect on heating patterns. Other recent works focused on microwave driven convection in pure liquids [9-11]. While the previous studies were based on pure liquids, we pay attention to a natural convection induced by microwave energy in a fluid-saturated porous medium.

Moreover, all the previous investigations above did not account for the effect of variable porosity in the vicinity of the impermeable wall. A region of higher porosity near the wall forms because the packing of the porous spheres near the column wall is not as efficient as that away

from the wall towards the column center [12]. Benenati and Brosilow [13] found a distinct porosity variation with a high porosity region close to the wall in packed beds. Values of porosity that are high close to an impermeable wall decrease to an asymptotic value at about four to five sphere diameters from it [14–15]. Many researchers found that the variation of porosity might significantly affect flow patterns as well as heat transfer features [13, 16 - 17]. The porosity of the bed exhibits sinusoidally damping decay especially at locations near wall [13]. This phenomenon leads to the channeling effect that could modify flow patterns significantly [14, 18 - 20]. Hsiao et. al. [17] have shown that including the effects of variable porosity and thermal dispersion on natural convection about the heated horizontal cylinder in an enclosed porous medium increases the average Nusselt number and reduces the error between the experimental data and their solutions. Thus, the effects of porosity variation should be taken into account in practice. [16, 21 - 23]

Therefore, in the present study herein we propose the numerical model for the microwave heating of a saturated porous packed bed in which the porosity variation is considered. The non-Darcian boundary and inertial effects are taken into account. Heating characteristic and flow pattern are numerically investigated. The numerical model is validated with an experimental data obtained using a rectangular waveguide operated under the microwave of TE_{10} mode.

2. EXPERIMENTAL SETUP

Figure 1 shows the experiment apparatus of microwave heating of saturated porous medium using a rectangular wave guide. The microwave system is a monochromatic wave of TE_{10} mode operating at a frequency of 2.45 GHz. From figure 1(b), magnetron (no.1) generates microwave and transmits along the z-direction of the rectangular wave guide (no.5) with inside cross-sectional dimensions of $109.2 \times 54.61 \text{ mm}^2$ that refers to a testing area (red circle) and a water load (no. 8) that is situated at the end of the wave guide. On the upstream side of the sample, an isolator is used to trap any microwave reflected from the sample to prevent damaging to the magnetron. The powers of incident, reflected and transmitted waves are measured by a wattmeter using a directional coupler (no. 6) (MICRO DENSHL, model DR-5000). Fiberoptic (no. 7) (LUXTRON Fluroptic Thermometer., model 790, accurate to $\pm 0.5^{\circ}$ C) is employed for temperature measurement. The fiberoptic probes are inserted into the sample, and situated on the XZ plane at Y = 25 mm. (see in Figure 2). Due to the symmetrical condition, temperatures are measured for only one side of plane. The samples are saturated porous packed beds that compose of glass beads and water. A container with a thickness of 0.75 mm is made of polypropylene which does not absorb microwave energy.

In our present experiment, a glass bead 0.15 mm in diameter is examined. The averaged (free stream) porosity of the packed bed corresponds to 0.385. The dielectric and thermal properties of water, air and glass bead are listed in Table 1.

3. MATHEMATICAL FORMULATION

3.1 Analysis of electromagnetic field

Since the electromagnetic field that is investigated is the microwave field in the TE_{10} mode, there is no variation of field in the direction between the broad faces of the rectangular wave guide and is uniform in the y-direction. Consequently, it is assumed that two dimension heat transfer model in x and z directions would be sufficient to identify the microwave heating phenomena in a rectangular wave guide [7]. The other assumptions are as follows:

- 1) The absorption of microwave by air in a rectangular wave guide is negligible.
- 2) The walls of rectangular wave guide are perfect conductors.
- The effect of sample container on the electromagnetic and temperature field can be neglected.

The proposed model is considered in TE_{10} mode so the Maxwell's equations can be written in term of the electric and magnetic intensities

$$\varepsilon \frac{\partial E_{y}}{\partial t} = \frac{\partial H_{x}}{\partial z} - \frac{\partial H_{z}}{\partial x} - \sigma E_{y} \tag{1}$$

$$\mu \frac{\partial H_z}{\partial t} = -\frac{\partial E_y}{\partial x} \tag{2}$$

$$\mu \frac{\partial H_x}{\partial t} = \frac{\partial E_y}{\partial z} \tag{3}$$

where E and H denote electric field intensity and magnetic field intensity, respectively. Subscripts x, y and z represent x, y and z components of vectors, respectively. Further, ε is the electrical permittivity, σ is the electrical conductivity and μ is the magnetic permeability. These symbols are

$$\varepsilon = \varepsilon_0 \varepsilon_r \tag{4}$$

$$\mu = \mu_0 \mu_r \tag{5}$$

$$\sigma = 2\pi f \varepsilon \tan \delta \tag{6}$$

When the material is heated unilaterally, it is found that as the dielectric constant and loss tangent coefficient vary, the penetration depth and the electric field within the dielectric material varies as well.

Since the dielectric properties of porous material depend on the functional temperature. The theory surrounding mixing formulas is used throughout in this study, in which the volume fractions of water liquid and glass particle are considered as follows: [24]

$$\varepsilon_r(T) = \varepsilon_r'(T) - j\varepsilon_r''(T) \tag{7}$$

where

$$\varepsilon_r'(T) = \phi \varepsilon_{rl}'(T) + (1 - \phi)\varepsilon_{rp}'$$
(8)

$$\varepsilon_{r}^{"}(T) = \phi \varepsilon_{rl}^{"}(T) + (1 - \phi)\varepsilon_{rp}^{"} \tag{9}$$

The loss tangent coefficient can be written as:

$$\tan \delta(T) = \frac{\varepsilon_r(T)}{\varepsilon_r(T)} \tag{10}$$

When the material is heated unilaterally, it is found that as the dielectric constant and loss tangent coefficient vary, the penetration depth and the electric field within the dielectric material

varies. The penetration depth is used to denote the depth at which the power density has decreased to 37 % of its initial value at the surface [25].

$$D_{p} = \frac{1}{2\pi f} \sqrt{\frac{\varepsilon_{r} \left(\sqrt{1 + \left(\frac{\varepsilon_{r}}{\varepsilon_{r}}\right)^{2} - 1}\right)}{2}} = \frac{1}{2\pi f} \sqrt{\frac{\varepsilon_{r} \left(\sqrt{1 + \left(\tan \delta\right)^{2} - 1}\right)}{2}}$$
(11)

where D_p is penetration depth, ε_r^* is relative dielectric loss factor. And v is microwave speed. The penetration depth of the microwave power is calculated according to equation (11), which shows how it depends on the dielectric properties of the material. It is noted that products with huge dimensions and high loss factors, may occasionally overheat a considerably thick layer on the outer layer. To prevent such phenomenon, the power density must be chosen so that enough time is provided for the essential heat transfer between boundary and core. If the thickness of the material is less than the penetration depth, only a fraction of the supplied energy will become absorbed. In example, consider the dielectric properties of water typically show moderate lousiness depending on the temperature. The water layer at low temperature typically shows slightly greater potential for absorbing microwaves. In the other words, an increase in the temperature typically decreases ε_r^* , accompanied by a slight increase in D_p .

The boundary conditions for TE_{10} mode can be formulated as follows:

1) Perfectly conducting boundary. Boundary conditions on the inner wall surface of wave guide are given by Faraday's law and Gauss's theorem:

$$E_{\parallel} = 0, H_{\perp} = 0 \tag{12}$$

where subscripts \parallel and \perp denote the components of tangential and normal directions, respectively.

2) Continuity boundary condition. Boundary conditions along the interface between sample and air are given by Ampere's law and Gauss's theorem:

$$E_{\parallel} = E_{\parallel}^{'}, H_{\parallel} = H_{\parallel}^{'} \tag{13}$$

3) Absorbing boundary condition. At both ends of rectangular wave guide, the first order absorbing conditions are applied:

$$\frac{\partial E_{y}}{\partial t} = \pm \upsilon \frac{\partial E_{y}}{\partial z} \tag{14}$$

where \pm is represented forward and backward direction and υ is velocity of wave.

4) Oscillation of the electric and magnetic intensities by magnetron. For incident wave due to magnetron is given by [7]

$$E_{y} = E_{yin} \sin\left(\frac{\pi x}{L_{x}}\right) \sin(2\pi f t) \tag{15}$$

$$H_{x} = \frac{E_{yin}}{Z_{H}} \sin\left(\frac{\pi x}{L_{x}}\right) \sin(2\pi f t)$$
 (16)

where E_{yin} is the input value of electric field intensity, L_x is the length of the rectangular wave guide in the x-direction, Z_H is the wave impedance defined as

$$Z_{H} = \frac{\lambda_{g} Z_{l}}{\lambda} = \frac{\lambda_{g}}{\lambda} \sqrt{\frac{\mu}{\varepsilon}}$$
 (17)

Here Z_l is intrinsic impedance depending on the properties of the material, λ and λ_g are the wave lengths of microwaves in free space and rectangular wave guide, respectively.

The power flux associated with a propagating electromagnetic wave is expressed by the Poynting vector:

$$s = \frac{1}{2} \operatorname{Re} (E \times H^*) \tag{18}$$

The Poynting theorem allows the evaluation of the microwave power input. It is represented as

$$P_{in} = \int_{A} S dA = \frac{A}{4Z_H} E_{yin}^2 \tag{19}$$

3.2 Analysis of temperature profile and flow field

The physical problem and coordinate system are depicted in Figure 3. The microwave is coming to the xy plane while the transport phenomena on the xz plane are currently investigated. To reduce complexity of the problem, several assumptions have been offered into the flow and energy equations.

- Corresponding to electromagnetic field, flow and temperature fields can be assumed to be two-dimensional plane.
- 2) The effect of the phase change is neglected.
- 3) Boussinesq approximation is used to account for the effect of density variation on the buoyancy force.
- 4) The surroundings of the porous packed bed are insulated except at the upper surface where energy exchanges with the ambient air.

3.2.1 Flow field equation

The porous medium is assumed to be homogeneous and thermally isotropic. The saturated fluid within the medium is in a local thermodynamic equilibrium (LTE) with the solid matrix [26 – 28]. The validity regime of local thermal equilibrium assumption has been established [29]. The fluid flow is unsteady, laminar and incompressible. The pressure work and viscous dissipation are all assumed negligible. The thermophysical properties of the porous medium are taken to be constant. However, the Boussinesq approximation takes into account of the effect of density variation on the buoyancy force. The Darcy-Forchheimer- Brinkman model was used to represent the fluid transport within the porous medium [29 – 30]. The Brinkmann's and the Forchheimer's extensions treats the viscous stresses at the bounding walls and the nonlinear drag effect due to the solid matrix respectively [30]. Furthermore, the solid matrix is made of spherical particles, while the porosity and permeability of the medium are varied depending on the distant from a wall. Using standard symbols, the governing equations describing the heat transfer phenomenon are given by

Continuity equation:

$$\frac{\partial u}{\partial x} + \frac{\partial w}{\partial z} = 0 \tag{20}$$

Momentum equations:

$$\frac{1}{\varepsilon} \frac{\partial u}{\partial t} + \frac{u}{\varepsilon^2} \frac{\partial u}{\partial x} + \frac{w}{\varepsilon^2} \frac{\partial u}{\partial z} = -\frac{1}{\rho_f} \frac{\partial p}{\partial x} + \frac{\upsilon}{\varepsilon} \left(\frac{\partial^2 u}{\partial x^2} + \frac{\partial^2 u}{\partial z^2} \right) - \frac{\mu u}{\rho_f \kappa} - F \left(u^2 + w^2 \right)^{1/2}$$
(21)

$$\frac{1}{\varepsilon} \frac{\partial w}{\partial t} + \frac{u}{\varepsilon^{2}} \frac{\partial w}{\partial x} + \frac{w}{\varepsilon^{2}} \frac{\partial w}{\partial z} = -\frac{1}{\rho_{f}} \frac{\partial p}{\partial z} + \frac{\upsilon}{\varepsilon} \left(\frac{\partial^{2} w}{\partial x^{2}} + \frac{\partial^{2} w}{\partial z^{2}} \right) - \frac{w\mu}{\rho_{f} \kappa} -F(u^{2} + w^{2})^{1/2} + g\beta (T - T_{0})$$
(22)

where ε , ν and β are porosity, kinematics viscosity and coefficient of thermal expansion of the water layer, respectively. The permeability κ and geometric F function are [16, 31]

$$\kappa = \frac{d_p^2 \varepsilon^3}{175(1-\varepsilon)^2} \tag{23}$$

$$F = \frac{1.75(1-\varepsilon)}{d_p \varepsilon^3} \tag{24}$$

The porosity is assumed to vary exponentially with a distance of wall [13, 15, 20]. Based on these previous studies, we proposed the variation of porosity within three confined walls of the bed; a bottom wall and two lateral walls. The expression that considers the variation of porosity in two directions in the xz plane is given by

$$\varepsilon = \varepsilon_s \left[1 + b \left\{ \exp\left(-\frac{bx}{dp} \right) + \exp\left(-\frac{b(W - x)}{dp} \right) + \exp\left(-\frac{bz}{dp} \right) \right\} \right]$$
 (25)

where d_p is the diameter of glass bead, ε_s known as a free-stream porosity is the porosity far away from walls, W is the width of packed bed and b and c are empirical constants. The dependencies of b and c to the ratio of the bed to bead diameter is small, and b and c were suggested to be 0.98 and 1.0 respectively [14].

3.2.2 Heat transfer equation

The temperature of liquid layer exposed to incident wave is obtained by solving the conventional heat transport equation with the microwave power absorbed included as a local electromagnetic heat generation term:

$$\sigma \frac{\partial T}{\partial t} + u \frac{\partial T}{\partial x} + w \frac{\partial T}{\partial z} = \alpha \left(\frac{\partial^2 T}{\partial x^2} + \frac{\partial^2 T}{\partial z^2} \right) + Q \tag{26}$$

where specific heat ratio $\sigma = \frac{\left[\varepsilon(\rho c_p)_f + (1-\varepsilon)(\rho c_p)_s\right]}{(\rho c_p)_f}$, $\alpha = k_e/(\rho c_p)_f$ is the thermal diffusivity.

The local electromagnetic heat generation term that is a function of the electric field and defined as

$$Q = 2\pi f \varepsilon_0 \varepsilon_r^{\dagger} \tan \delta (E_y)^2 \tag{27}$$

Boundary and initial conditions for these equations:

Since the walls of container are rigid, the velocities are zero. At the interface between liquid layer and the walls of container, zero slip boundary conditions are used for the momentum equations.

1) At the upper surface, the velocity in normal direction (w) and shear stress in the horizontal direction are assumed to be zero, where the influence of Marangoni flow [7] can be applied:

$$\eta \frac{\partial u}{\partial z} = -\frac{d\xi}{dT} \frac{\partial T}{\partial x} \tag{28}$$

2) The walls, except top wall, are insulated so no heat and mass exchanges:

$$\frac{\partial T}{\partial x} = \frac{\partial T}{\partial z} = 0 \tag{29}$$

3) heat is lost from the surface via natural convection and radiation:

$$-\lambda \frac{\partial T}{\partial z} = h_c (T - T_{\infty}) + \sigma_{rad} \varepsilon_{rad} (T^4 - T_{\infty}^4)$$
(30)

4) The initial condition of a medium is defined as:

$$T = T_0 \text{ at } t = 0 \tag{31}$$

4. NUMERICAL PROCEDURE

The description of heat transport and flow pattern of liquid layer equations (20)-(24) and (26) requires specification of temperature (T), velocity component (u, w) and pressure (p). These equations are coupled to the Maxwell's equations (equation (1)-(3)) by equation (27). It represents the heating effect of the microwaves in the liquid-container domain.

4.1 Electromagnetic equations and FDTD discretization

The electromagnetic equations are solved by using FDTD method. With this method the electric field components (E) are stored halfway between the basic nodes while magnetic field components (H) are stored at the center. So they are calculated at alternating half-time steps. E and H field components are discretized by a central difference method (second-order accurate) in both spatial and time domain.

4.2 Fluid flow and heat transport equations and finite control volume discretization

Equations (20)-(24) are solved numerically by using the finite control volume along with the SIMPLE algorithm developed by Patankar. The reason to use this method is advantages of flux conservation that avoids generation of parasitic source. The basic strategy of the finite control volume discretization method is to divide the calculated domain into a number of control volumes and then integrate the conservation equations over this control volume over an interval

of time $[t,t+\Delta t]$. At the boundaries of the calculated domain, the conservation equations are discretized by integrating over half the control volume and taking into account the boundary conditions. At the corners of the calculated domain we used a quarter of control volume. The fully Euler implicit time discretization finite difference scheme is used to arrive at the solution in time. Additionally, the details about numerical discretization of this method can be found in the recent literature.

4.2.1 The stability and accuracy of calculation

The choice of spatial and temporal resolution is motivated by reasons of stability and accuracy. To ensure stability of the time stepping algorithm Δt must be chosen to satisfy the courant stability condition and defined as

$$\Delta t \le \frac{\sqrt{(\Delta x)^2 + (\Delta z)^2}}{\upsilon} \tag{32}$$

and the spatial resolution of each cell, defined as

$$\Delta x, \Delta z \le \frac{\lambda_g}{10\sqrt{\varepsilon_r}} \tag{33}$$

Corresponding to equation (32) and (33), the calculation conditions are as follows:

- 1) Grid size: $\Delta x = 1.0922$ mm and $\Delta z = 1.0000$ mm
- 2) Time steps: $\Delta t = 2 \times 10^{-12}$ s and $\Delta t = 0.01$ s are used corresponding to electromagnetic field and temperature field calculations, respectively.
- 3) Relative error in the iteration procedures of 10⁻⁶ was chosen.

4.2.2 The iterative computational schemes

Since the dielectric properties of liquid layer samples are temperature dependent, to understand the influence of electromagnetic field on microwave heating of liquid layer realistically, it is necessary to consider the coupling between electric field and temperature and fluid flow fields. For this reason, the iterative computational schemes are required to resolve the coupled non-linear Maxwell's equations, momentum and heat transport equations.

The computational scheme is to first compute a local heat generation term by running an electromagnetic calculation with uniform properties determined from initial temperature data. The electromagnetic calculation is performed until a sufficient period is reached in which representative average rms (root mean square) of the electric field at each point is computed and used to solve the time dependent temperature and velocities field. Using these temperatures new values of the dielectric properties are calculated and use to re-calculate the electromagnetic fields and then the microwave power absorption. All the steps are repeated until the required heating time is reached.

5. RESULTS AND DISCUSSION

In the present simulations, the formulation that computes the variation of porosity in two directions given by equation (25) is employed to describe the two-dimensional porosity variation. The glass bead diameters of 1.0 mm and 3.0 mm are examined with which the free-stream porosity is 0.385. The resulting calculations are illustrated in figure 4 on the x-z plane. Variations of the bed porosity were considered since it was proved that the porosity decayed from the wall [13 - 14]. As clearly seen in the figure, the porosity is high in the vicinity of an

impermeable boundary and reduces to a free-stream value at about four to five bead diameters from the boundary [15]. The computed porosities vary accounting to the distances from the walls in two directions. Porosities are largest at the corners because it is not efficient to pack spherical beads at bed corners. The gradients of porosity are found lower with larger particle diameter.

To examine the validity of the mathematical model, the numerical results were compared with the experimental data. The description with regard to the experimental setup and associated parameters is given in section 2. The diameter of glass beads and free-stream porosity are 0.15 mm and 0.385 respectively. With respect to the model simulation, the computed data, for both uniform and non-uniform, cases were extracted at 30 and 50 seconds. The comparisons of temperature distributions on the x-z plane at the horizontal line z = 21 mm are shown in Figure 5 and Figure 6 at 30 and 50 seconds respectively. The results show an appreciably improved agreement when variation of porosity within the packed bed is considered. For the uniform case, the peak temperature is about 40 °C at 30 seconds, and reaches 50 °C at later time while temperatures are lower in the case of variable porosity. However, it is clear in both the figures that temperature is highest at the middle location since the density of the electric field in the TE10 mode is high around the center region in the wave guide.

Figure 7 displays temperature contours as a function of time of the two cases which exhibit a wavy behavior corresponding to the resonance of electric field. For the non-uniform porosity, the heating rate is noticeably slower than that for the uniform porosity. The reason behind this is that in the non-uniform porosity medium, more water content exists near the bottom wall attributed to a higher water-filled pore density. Since water is very lossy, large amount of energy can be absorbed as both the incoming waves and the reflected waves attenuate especially at the bottom area. This occurrence results in a resonance of weaker standing wave

with smaller amplitude throughout the packed bed. The weaker standing wave dissipates less energy which is in turn converted into less thermal energy, giving relatively slow heating rate. This explains why non-uniform porous gives overall lower temperature. Furthermore, more amount of water present in the non-uniform medium causes a smaller depth of penetration since water has relatively high values of dielectric constant and high loss tangent. Figure 8 shows variation of centerline temperature vertically along the z axis at the different times of the two bed types. The resulting plots confirm wavy behavior shown in figure 7. Moreover, it is obvious that the bed temperature is higher in the uniform-porosity porous bed.

In terms of flow characteristic, the instantaneous velocity vectors at 60 seconds are displayed in figure 9. The fluid flows as it is driven by the effect of buoyancy that overcomes the retarding viscous force. The non-uniform temperature distribution evident in figure 7 leads to an unstable condition. Temperature gradients which exist in both transverse and axial directions result in circulated flows. The velocities are higher close to the top boundary since there exist higher temperature gradients thereby higher density gradients leading stronger buoyancy-induced flows. It is seen that flow velocities in the variable-porosity medium are lower than those in the uniform-porosity medium. This result is attributed to higher porosities near walls in the non-uniform case. Higher porosity medium corresponds to higher permeability which allows greater flow velocity due to smaller boundary and inertial effects. The difference is clear in the vicinity of walls where high velocities carry energy from the wall towards the inner area.

To gain more insight in flow phenomena, the centerline velocity magnitudes along the x direction are depicted in figure 10. It is clear that the non-uniform porosity gives larger magnitudes. Two peaks are seen spatially in both the cases. The peak values are at the same locations as observed in figure 9. More importantly, the gradient of magnitude is larger in the

non-uniform case due to the presence of porosity gradients. It is worthwhile comparing a u-component velocity shown in figure 11 along the x axis. The sign of the value reflects flow directions along the x axis. Relatively cold fluid flows towards the center domain from both sides to replace a hot fluid portion that expands towards the top boundary. This result is consistent to the flow behaviors depicted in figure 9.

6. CONCLUSIONS

The microwave heating of a porous medium with a non-uniform porosity is carried out, based on the proposed numerical model. The two-dimensional variation of porosity of the medium is considered to be a function of the distant from the bed walls. The transient Maxwell's equations are employed to solve for the description of the electromagnetic field in the wave guide and medium. The generalized non-Darcian model that takes into account of the presence of a solid drag and the inertial effect is included. The numerical results are in a good agreement with the experimental data. In addition to the effect on the convective flow velocity that is larger in the non-uniform case, it is found that the variation of porosity near the wall has an important influence on the dielectric properties of the porous packed bed that affect the heating process markedly.

7. ACKNOWLEDGEMENTS

The authors are grateful for the financial support provided by the Thailand Research Fund under Contract No. MGR5180238.

REFERENCES

- [1] W. K. Chen, H. T. Davis, E. A. Davis, G. Joan, Heat and Mass Transfer in Water-Laden Sandstone: Microwave Heating, AIChE Journal 31 (5) (1985) 842-848.
- [2] H. Ni, A. K. Datta, K. E. Torrance, Moisture transport in intensive microwave heating of biomaterials: porous media model, International J. Heat and Mass Transfer 42 (1999) 1501-1512.
- [3] H. Feng, J. Tang, R. P. Cavalieri, O. A. Plumb, Heat and mass transport in microwave drying of porous materials in a spouted bed, AIChE Journal 47 (2001) 1499-1512.
- [4] P. Ratanadecho, K. Aoki, M. Akahori, Influence of Irradiation Time, Particle Sizes, and Initial Moisture Content During Microwave Drying of Multi-Layered Capillary Porous Materials, Journal of Heat Transfer 124 (1) (2002) 151-161.
- [5] D. D. Dinčov, K. A. Parrot, K. A. Pericleous, Heat and Mass transfer in two-phase porous materials under intensive microwave heating, Journal of Food Engineering 65 (2004) 403-412.
- [6] P. Ratanadecho, The simulation of microwave heating of wood using a rectangular wave guide: Influence of frequency and sample size, Chemical Engineering Science (61) (2006) 4798-4811.
- [7] P. Ratanadecho, K. Aoki, M. Akahori, A numerical and experimental investigation of modelling of microwave heating for liquid layers using a rectangular wave guide (effects of natural convection and dielectric properties), Applied Mathematical Modelling 26 (2002) 449-472.
- [8] W. Cha-um, P. Rattanadecho, W. Pakdee, Experimental Analysis of Microwave Heating of Dielectric Materials Using a Rectangular Wave Guide (MODE: TE₁₀) (Case study: water layer and saturated porous medium), Experimental Thermal and Fluid Science 33(3) (2009) 472-481.

- [9] K. G. Ayappa, S. Brandon 1994, Microwave driven convection in a square cavity, AIChE Journal 40 (7) (1994) 1268-1272.
- [10] A. S. Franca, K. Haghighi, Adaptive finite element analysis of microwave driven convection, International Communications in Heat and Mass Transfer 23(2) (1996) 177-186.
- [11] S. Chatterjee, T. Basak, S. K. Das, Microwave driven convection in a rotating cylindrical cavity: A numerical study, Journal of Food Engineering 79 (2007) 1269-1279.
- [12] S. Lui, J. Masliyah, Single fluid flow in porous media, Chemical Engineering Communications 148 (1996) 653-732.
- [13] R. F. Benenati, C. B. Brosilow, Void fraction distribution in pack beds AIChE Journal, 8 (1962) 359-361.
- [14] K. Vafai, Convective flow and heat transfer in variable-porosity media, Journal of Fluid Mechanics 147 (1984) 233-259.
- [15] A. Amiri, K. Vafai, Analysis of dispersion effects and non-thermal equilibrium, non-Darcian, variable porosity incompressible flow through porous media, International Journal of Heat and Mass Transfer 37 (6) (1994) 939-954.
- [16] A. K. Abdul-Rahim, A. J. Chamkha, Variable porosity and thermal dispersion effects on coupled heat and mass transfer by natural convection from a surface embedded in a non-metallic porous medium, International Journal of Numerical Methods for Heat & Fluid Flow 11 (5) (2001) 413-429.
- [17] S. W. Hsiao, P. Cheng, C. K. Chen, Non-uniform porosity and thermal dispersion effects on natural convection about a heated horizontal cylinder in an enclosed porous medium, International Journal of Heat and Mass Transfer 35 (12) (1992) 3407-3418.

- [18] K. Vafai, Analysis of the channeling effect in variable porosity media, Journal of Energy Resources Technology 108 (1986) 131-139.
- [19] M. L. Hunt, C. L. Tien, Non-Darcian convection in cylindrical packed beds, Journal of Heat Transfer 110 (1998) 2523-2532.
- [20] D. Poulikakos, K. Renken, Forced convection in a channel filled with porous medium, including the effects of flow inertia, variable porosity and Brinkman frction. ASME Journal of Heat Transfer 109 (1987) 880-888.
- [21] H. Shih-Wen, P. Cheng, C. Chao-Kuang, Non-uniform porosity and thermal dispersion effects on natural convection about a heated horizontal cylinder in an enclosed porous medium International Journal of Heat and Mass Transfer 35 (12) (1992) 3407-3418.
- [22] Z. Chai, Z. Guo, Study of electro-osmotic flows in microchannels packed with variable porosity media via lattice Boltzmann method, Journal of Applied Physics 101 (2007) 104913.
- [23] S. Akbal, F. Baytas, Effects of non-uniform porosity on double diffusive natural convection in a porous cavity with partially permeable wall, International Journal of thermal Sciences 47 (7) (2008) 875-885.
- [24] P. Ratanadecho, K. Aoki, M. Akahori, Experimental and Numerical study of microwave drying in unsaturated porous material, International Communications in Heat and Mass Transfer 28 (5) (2001) 605-616.
- [25] P. Rattanadecho, The simulation of microwave heating of wood using a rectangular wave guide: Influence of frequency and sample size, Chemical Engineering Science 61 (2006) 4798-4811.
- [26] M. M. El-Refaee, M. M. Elsayed, N. M. Al-Najem, A. A. Noor, Natural convection in partially cooled tilted cavities, International Journal of Numerical Methods 28 (1998) 477-499.

- [27] D. A. Nield, A. Bejan, Convection in Porous Media, Springer, New York, USA. 1999.
- [28] A. A. Al-Amiri, Natural convection in porous enclosures: The application of the two-energy equation model, Numerical Heat Transfer Part A 41 (2002) 817-834.
- [29] Marafie A, Vafai K. Analysis of non-Darcian effects on temperature differentials in porous media. Int. J. Heat Mass Transfer 2001; 44:4401-4411.
- [30] P. Nithiarasu, K. N. Seetharamu, T. Sundararajan, Natural convective heat transfer in a Fluid Saturated variable porosity medium, International Journal of Heat and Mass Transfer 40 (1996) 3955-3967.
- [31] A. J. Chamkha, C. Issa, K. Khanafer, Natural convection from an inclined plate embedded in a variable porosity porous medium due to solar radiation, International Journal of thermal Sciences 41 (2002) 73-81.

List of Figure Captions

- Figure 1. The microwave heating system with a rectangular wave guide.
- Figure 2. Locations of temperature measurement in symmetrical xz plane.
- Figure 3. Schematic of the physical problem.
- Figure 4. Porosity distributions with the bead diameters: (a) 1 mm and (b) 3 mm.
- Figure 5. The temperature distributions taken at 30 seconds are shown as to compare the numerical solutions with the experimental result.
- Figure 6. The temperature distributions taken at 50 seconds are shown as to compare the numerical solutions with the experimental result.
- Figure 7. Time evolutions of temperature contour within the porous bed at 20, 40 and 60 seconds for uniform case (a-c) and non-uniform case (d-f).

- Figure 8. Centerline temperature along the z axis for uniform (dashed line) and non-uniform (solid line) porous packed bed.
- Figure 9. Velocity vectors from the two cases of porous medium; (a) Non-uniform (b) Uniform.
- Figure 10. Variations of velocity magnitudes along the x axis for uniform (dashed line) and non-uniform (solid line) porous packed bed.
- Figure 11. Variations of u-component velocity along the x axis for uniform (dashed line) and non-uniform (solid line) porous packed bed.

Figures

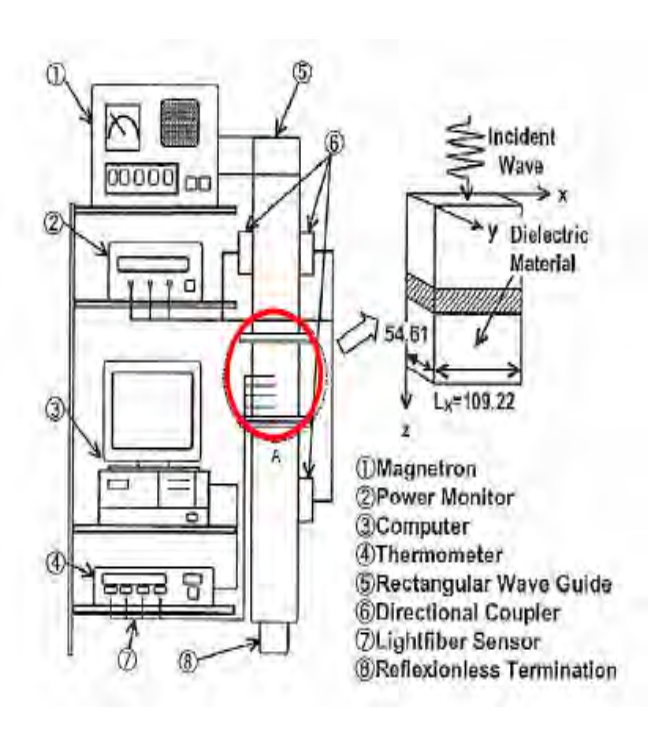


Figure 1

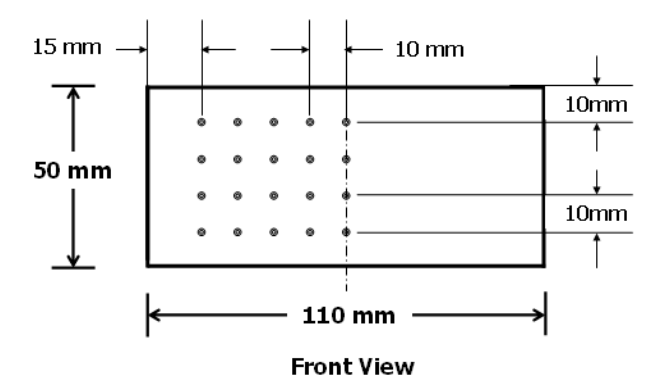


Figure 2

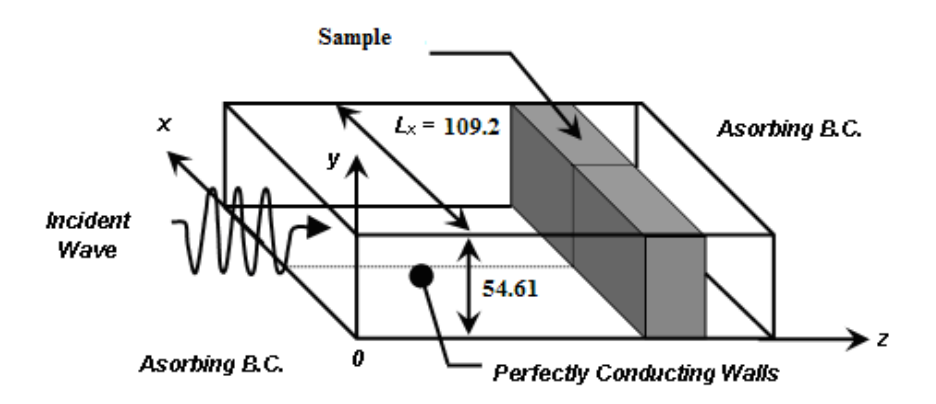


Figure 3

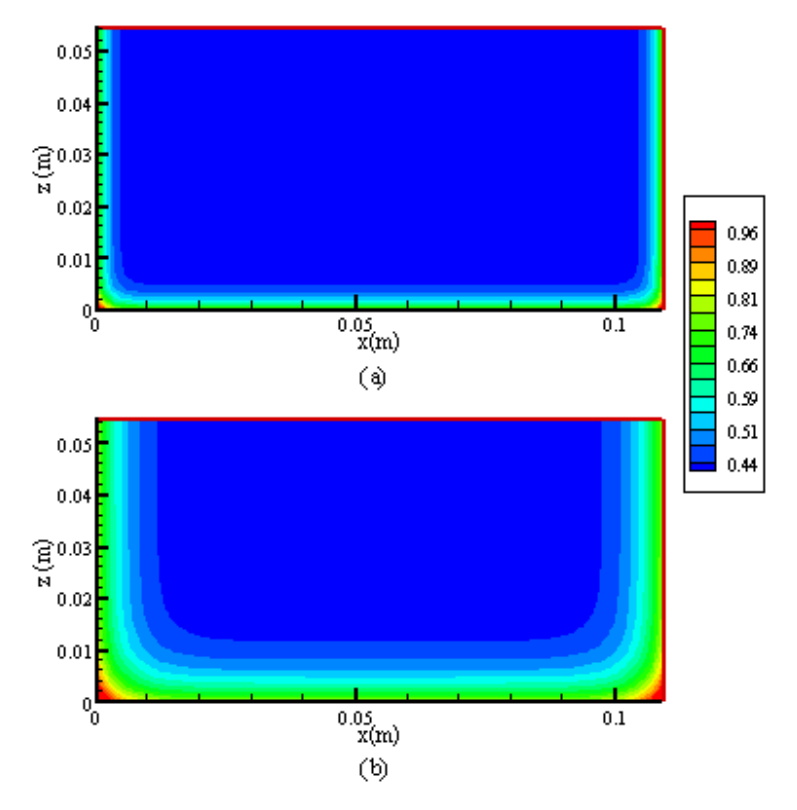
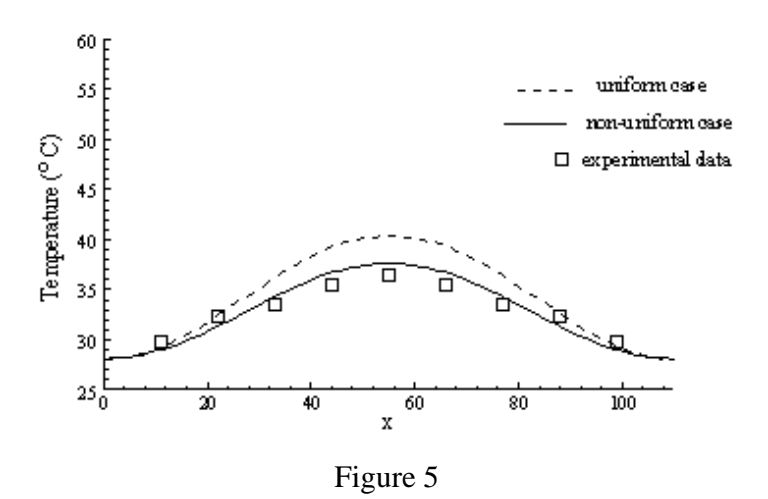


Figure 4



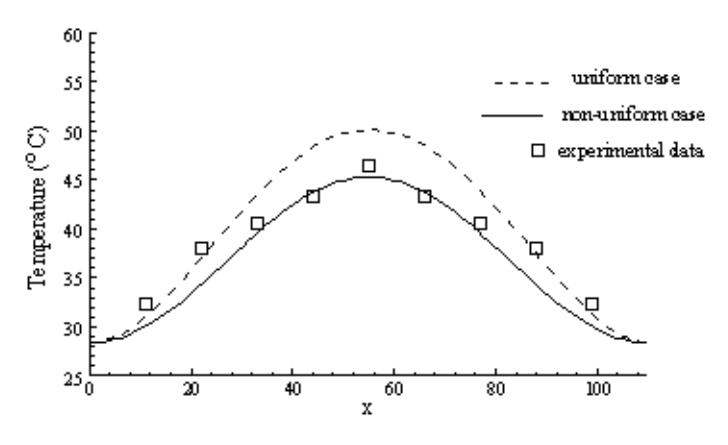


Figure 6

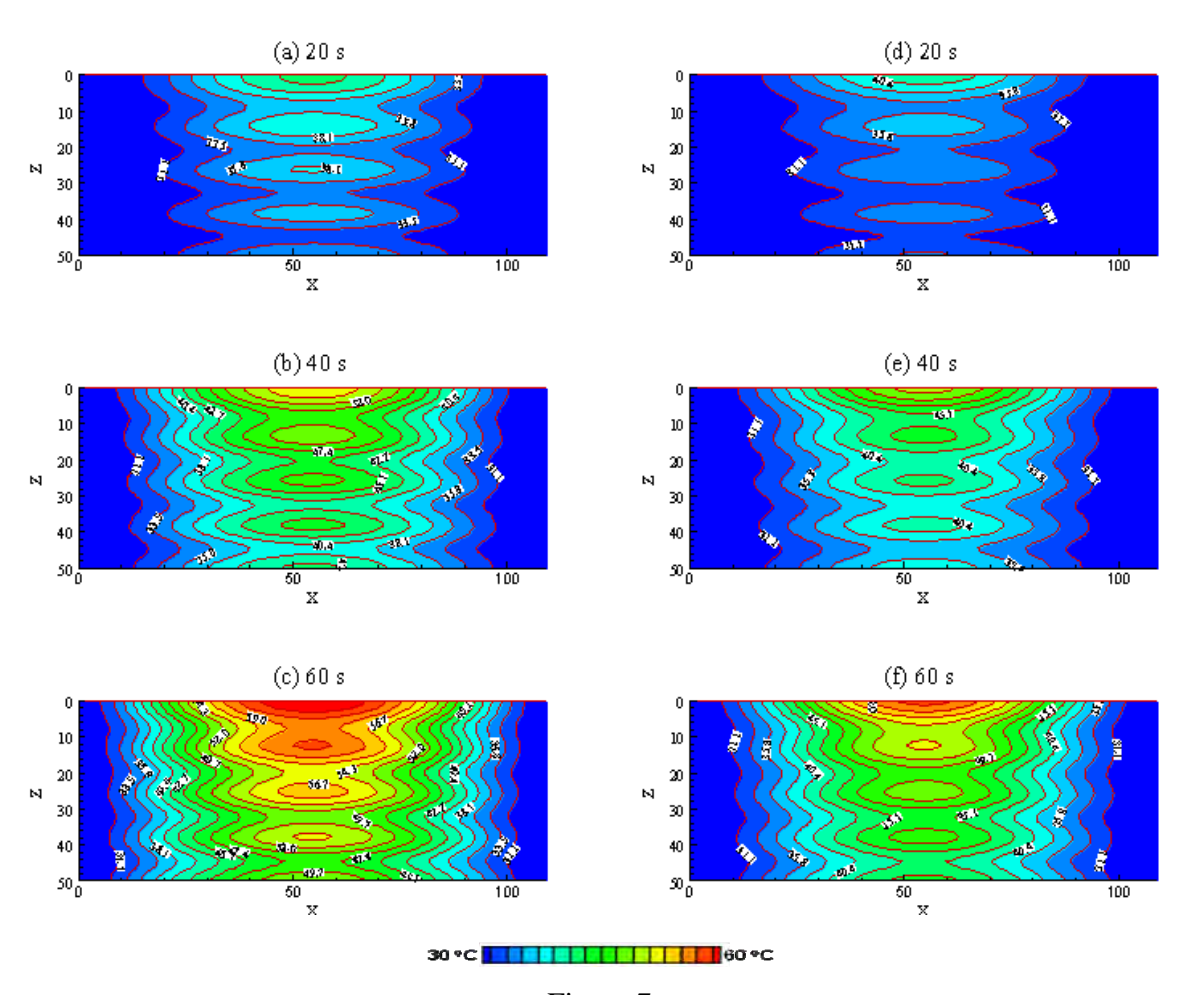


Figure 7

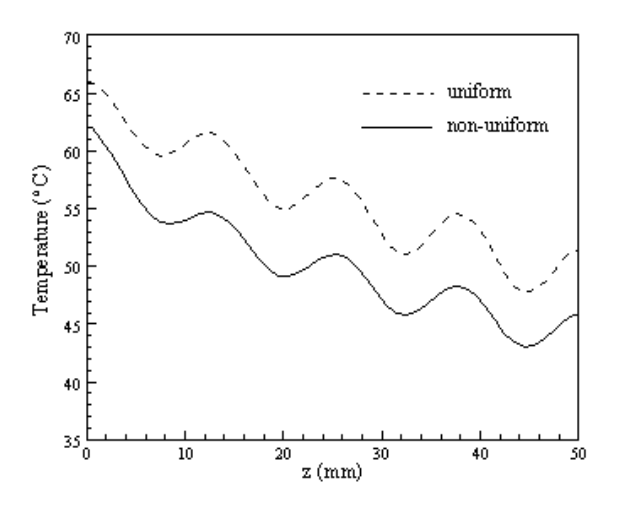


Figure 8

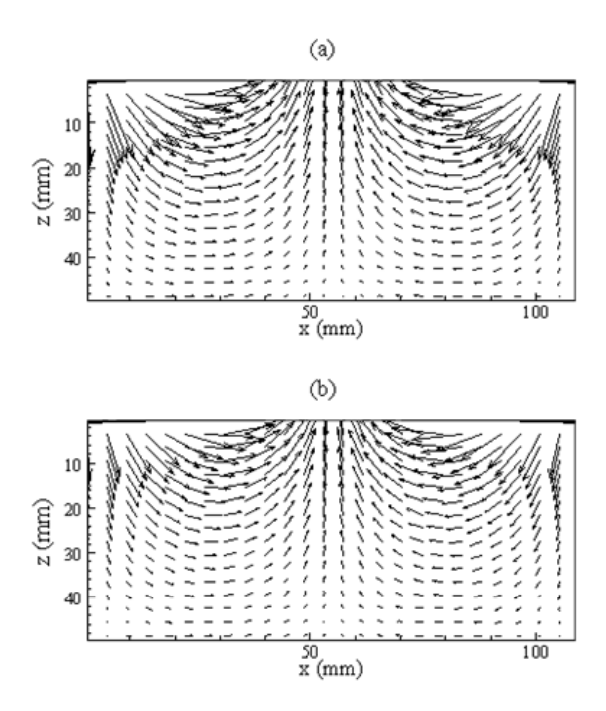


Figure 9

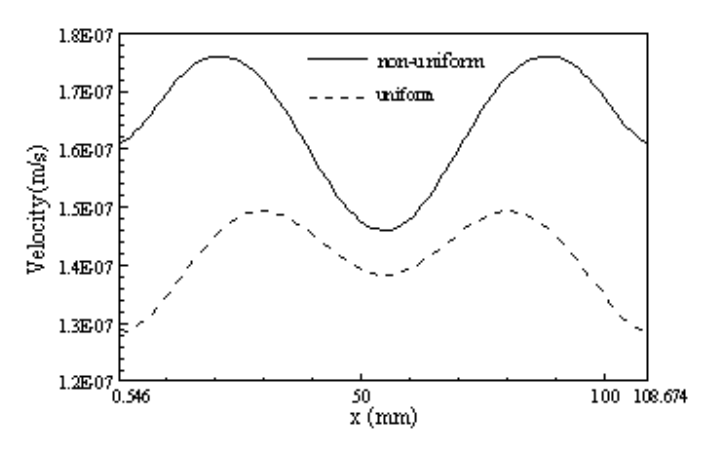


Figure 10

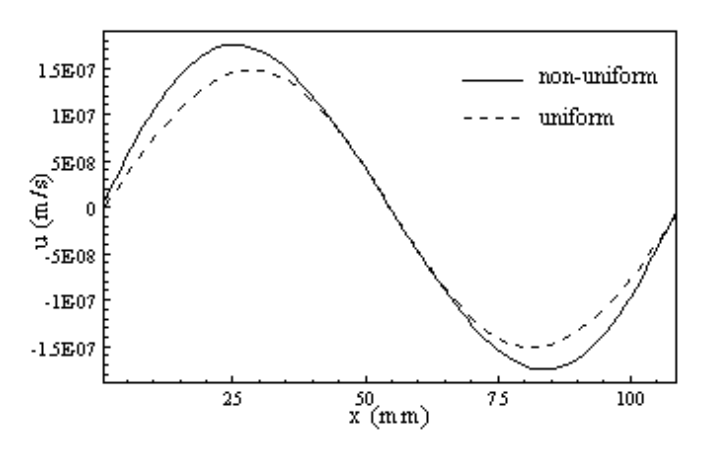


Figure 11

Table 1 The electromagnetic and thermo physical properties used in the computations [24]

<u>Table</u>

Property	water	Glass bead
Heat capacity, $C_p(Jkg^{-1}K^{-1})$	4190	800
Thermal conductivity, $\lambda (Wm^{-1}K^{-1})$	0.609	1.0
Density, $\rho(kgm^{-3})$	1000	2500
Dielectric constant 1 , $\mathcal{E}_{r}^{'}$	$88.15\text{-}0.414T + (0.131 \times 10^{-2})T^2 - (0.046 \times 10^{-4})T^3$	5.1
Loss tangent ¹ , $\tan \delta$	0.323 - (9.499×10^{-3}) T+ (1.27×10^{-4}) T ² - (6.13×10^{-7}) T ³	0.01

¹T is in °C.